5 Physics Aspects of Charge Migration Through DNA

Vadim Apalkov[1], Xue-Feng Wang[2], and Tapash Chakraborty[2]

[1] Department of Physics and Astronomy, Georgia State University, Atlanta, Georgia 30303, USA
[2] Department of Physics and Astronomy, University of Manitoba, Winnipeg, Canada R3T 2N2
tapash@physics.umanitoba.ca

5.1 Introduction

As the scientific activities of the biology, chemistry, and physics communities meet at the nanometer scale, interdisciplinary works are the most efficient avenues to explore many mysteries in science and technology that has been appreciated only in recent decades. One of these mysteries is a deeper understanding and efficient manipulation of charge migration in DNA. Charge migration or the redox process in DNA is directly related to the damage and repair of DNA occurred in the cells of human beings [1]. As we know now, the DNA damage is responsible for many neurological diseases, and plays an important role in aging and many forms of human cancer. On the other hand, molecular electronic devices are believed to be the most promising technology in the near future. DNA has the property of self-assembly and DNA based devices have the advantage of large-scale industrial production. Construction of the artificial DNAs and understanding of charge migration in them then become crucially important [2,3]. Furthermore, DNA sequencing, the process of deciphering the exact order of the 3 billion base pairs that make up the DNA of 24 different chromosomes, has the potential to revolutionize exploration of human biology and medicine. Currently the main concern here is the efficiency of the sequencing process. Study of the transverse charge transport in DNA may result in an efficient tool for rapid DNA sequencing [4, 5] as well as fundamental understanding of charge migration across the DNA. In the last decade, charge migration in molecules and DNA has been addressed by many authors which has established a basis for further developments in this field [2, 3, 6–17]. In this chapter, we investigate some aspects of it from a physical point of view.

5.2 DNA Model for Charge Migration

5.2.1 Molecular Structure

DNA (deoxyribonucleic acid) is the molecule responsible for the storage of genetic information in the cells. The primary structure of DNA as shown in

Fig. 5.1 consists of two chain polymers of the nucleotide units, and is called the DNA duplex. Each nucleotide contains three components: a heterocyclic base, a deoxyribose sugar (pentose), and a phosphate (phosphoric acid). The sugar and phosphate of the successive nucleotide units along each chain are connected in an alternating sequence and form the backbone of the chain. The base of each nucleotide attaches to the sugar on one side and to its counterpart base from the other chain on the other side. The two chains are held together through pairing of their bases by hydrogen bonds. There are four kinds of bases, two purine derivatives, guanine (G) and adenine (A), and two pyrimidine derivatives, cytosine (C) and thymine (T). The pairing occurs only between G and C by three hydrogen bonds or between A and T by two hydrogen bonds, i.e. there are only two kinds of base pairs, (G:C) and (A:T). Along each backbone, the phosphate connects the carbon 5′ of one sugar with the carbon 3′ of the next sugar (Fig. 5.1a) [18].

The secondary structure of DNA is a double helix with the duplex nucleotide strands twisted around each other. The two strands of the nucleotide polymer in a DNA are oriented in opposite directions, one from carbon 5′ to 3′ and the other from carbon 3′ to 5′ [18]. The antiparallel orientation helps to align the hydrogen bond donors and acceptors. Along the double helix, the two strands of the backbone wrap around the stacked base-pair layers. There are three classes of structures, called the B, A, and the Z forms. The form of the B-DNA commonly exists in living beings where the environment is humid. Its helix is about 2 nm in diameter with a vertical distance of about 0.34 nm between layers of the base pairs and about 10 base pairs for each complete turn of the helix (Fig. 5.1b). This is the prototype of DNA for many theoretical works including this work.

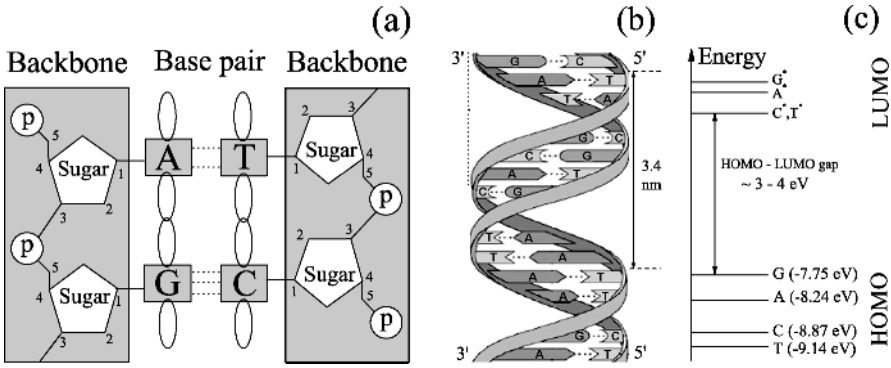

Fig. 5.1. a The primary structure of a DNA duplex with four nucleotides. The elliptical loops show the overlap of the π bonds along the base stacking direction; the *dashed lines* between the (G:C) and (A:T) base pairs are the hydrogen bonds; the numbers around each sugar denote the numbers of the sugar carbons. **b** The DNA double helix. **c** Illustration of the π bond HOMO energies and π^* bond LUMO energies of the G, C, A, T bases

From the viewpoint of quantum mechanics, the charge migration in DNA occurs via electronic transitions among states near the chemical potential. The characteristics of charge transfer is then mainly determined by the properties of the highest occupied molecular states (HOMO) and the lowest unoccupied molecular states (LUMO) of the nucleotide in the cases of hole transfer and electron transfer respectively. At zero temperature the chemical potential separates the LUMO from the HOMO. In Fig. 5.1c, the HOMO and LUMO energy levels for the bases G, A, T, and C are also illustrated (approximately). In a DNA with all the bases present, the HOMO-LUMO gap is about 3 – 4 eV but the exact value is still an open question [13,19–21]. The HOMO and LUMO states are mainly composed of molecular states of the π and π^* bonds, i.e. the p_z orbits of the carbon-carbon double bonds, in the purine and pyrimidine bases. The wave function overlap of the π (π^*) bonds between the neighboring bases allows holes (electrons) to jump from one base to another and results in the charge migration along the DNA duplexes.

5.2.2 The Tight-Binding Model

In order to describe the charge migration in DNA quantitatively, both microscopic and macroscopic models have been reported in the literature [7]. In the former case, the system is handled via the first principle; the outer-shell orbits of all atoms in the system and the coupling between them are taken into account explicitly and the transport properties of the system are obtained by the *ab initio* calculations. For the macroscopic models, crucial physical information is extracted from the *ab initio* calculations and are parameterized to simplify the system in the hope of being able to handle bigger systems and also obtain more physical insights than those available from the *ab initio* calculations.

Based on the existing experiments and the *ab initio* results, it has been suggested that the charge migration in DNA is a hole transport via the HOMO states of the bases and the energy gap between the HOMO and LUMO states in each base is about 4 eV [13]. In the zeroth order approximation for a macroscopic model, the system is composed of a series of sites where each site corresponds to a HOMO state of a base. A tight-binding model of the hole transport can then be established with on-site energies for the HOMO energies of the bases and the coupling parameters between the sites for coupling of the HOMO states between the bases.

The on-site energy of each base is then the energy to create a hole in the HOMO state of the base, viz., the ionization energy. The ionization energy is sensitive to the existence of other bases around and also to the environment. This value for the single bases can be calculated by the quantum chemical *ab initio* methods and were confirmed by measurements in the bases' gas phase. The calculated HOMO hole energies for the isolated single bases G, C, T, and A are $E_G = 7.75$, $E_C = 8.87$, $E_T = 9.14$, and $E_A = 8.24$ eV respectively [19, 20, 22, 23]. It is to be noted that these values may depend

on the method used [24]. Just as for the on-site energies of the bases, the coupling parameters between different sites (bases) in principle, can also be calculated by the *ab initio* methods. Usually, this effective coupling parameter depends on how the macroscopic model is established. While the intrinsic value comes from the overlap of the π orbit wave functions between the bases, the effective one should be adjusted if other factors (see below) are not explicitly taken into account in the macroscopic tight-binding model. Until now, the calculated coupling parameter from different *ab initio* models are very scattered in a range of $0.01 - 0.4\,\mathrm{eV}$ [19, 25, 26]. Nevertheless, some common qualitative characteristics of the coupling have been extracted from these calculations. Although the purine and pyrimidine bases within each Watson-Crick base pair are strongly coupled by the hydrogen bonds [27], the hydrogen bonds do not participate in the carrier transport because they have a lower energy than the HOMO states. As a result, the interstrand coupling parameter for the HOMO states between them is much weaker than the intrastrand coupling parameter between the neighboring bases along the DNA strands [25, 26]. Because the π bond is highly anisotropic, the coupling parameters are sensitive to the relative position of the two bases in question and a twist of the DNA duplex may modify the coupling parameters significantly [13].

In the above primary picture of the system, we have neglected some other factors which can affect the charge transfer in DNA. In reality, the HOMO states of the bases are not isolated from but are coupled to the other components of the system. First, the HOMO state in a base is coupled to the other outer-shell electronic states with lower or higher energies. The hydrogen bonds, for example, can influence the HOMO states [28]. Second, it is coupled to the inner-shell electronic states and the nuclear states, which introduce the electron-phonon or vibronic coupling [11]. Third, it is coupled to the electronic states in the backbone [29]. Fourth, the charge transfer is affected by the environment, including the static and dynamic screening and random impurities [11]. Fifth, when a finite potential bias is applied over the system, the modification of the potential profile along the DNA duplex and other nonlinear effects will become important [30]. Sixth, spin effects may also be important in some situations [31–33]. Finally, if there is more than one hole present in the DNA, correlation between them may play an important role in the behavior of the charge migration in the system [34].

Different strategies are used to handle these factors. Obviously, a complete and straightforward way would be to take all of these factors into account explicitly. However, this is not very practical because few of these factors are well studied and the corresponding parameters are far from being established. A model with too many uncertain parameters will be confusing and useless. Fortunately, from the mathematical point of view, many characters of these factors can be integrated into the renormalized on-site energy or the coupling parameter. In some cases, even the on-site energy and the coupling parameter

can in turn, be represented by each other [35]. Based on this fact, in the numerical calculation of this work, we have used the fixed HOMO energies of the isolated single bases as the on-site energies but leave the effective coupling parameters flexible. However, to which extent and under which condition the parameterization process is valid are still subject of further theoretical and experimental studies.

In the following, we shall discuss only the distance dependence of the charge transfer and neglect the reorganization energetics involved in the charge transfer process, which affects mainly the temperature dependence [11, 16, 36].

5.3 Evaluation of the Electron Transfer Rate in a Chain Model

5.3.1 The One-Dimensional Chain Model

In the simplest single-particle tight-binding model, we assume that the system can be parameterized into a chain model in which an effective on-site energy is used for the HOMO energy of each base pair and an effective coupling parameter between any two nearest neighbor sites [37]. For a homogeneous DNA duplex, such as the Poly(G:C) polymers, this model should be very effective because the charge migration occurs along the purine strand in case of the hole transport.

In the chain model, the Hamiltonian of a N-base-pair DNA as shown in Fig. 5.2a reads

$$\mathcal{H}_{\mathrm{DNA}} = \sum_{n=1}^{N} \varepsilon_n c_n^{\dagger} c_n - \sum_{n=1}^{N-1} t_{n,n+1} (c_n^{\dagger} c_{n+1} + c_{n+1}^{\dagger} c_n)] \; . \tag{5.1}$$

Here, $c_n^{\dagger}$ is the creation operator of holes on site n of the DNA chain (for $1 \leq n \leq N$) and $-t_{n,n+1}$ is the coupling parameter between nearest neighbor sites n and $n+1$ [38]. In this tight-binding model, the creation operator $c_n^{\dagger}$ corresponds to the local electronic state $|n\rangle$ on site n and we assume that all the states are orthogonal to each other, i.e. $\langle m|n\rangle = \delta_{m,n}$ with $\delta_{m,n}$ the Kronecker delta function. In the matrix form, the secular equation then reads $|\hat{\mathcal{H}}_{\mathrm{DNA}} - E\hat{I}| = 0$ with $\hat{I}$ the unit matrix. In a real DNA, the HOMO states, $|\tilde{n}\rangle$, of different bases are not orthogonal to each other and the overlap matrix $\hat{S}$ with elements $S_{m,n} = \langle \tilde{m}|\tilde{n}\rangle$ is not the unit matrix. As a result, the secular equation should be $|\hat{\mathcal{H}}_{\mathrm{DNA}} - E\hat{S}| = 0$. Here an orthogonalization process is assumed to have been done to transform the HOMO molecular states $|\tilde{n}\rangle$ to the on-site states $|n\rangle$ and to construct the site representation of the DNA system [39]. The Hamiltonian is transformed accordingly but the modification to the on-site energy by the orthogonalization process is neglected.

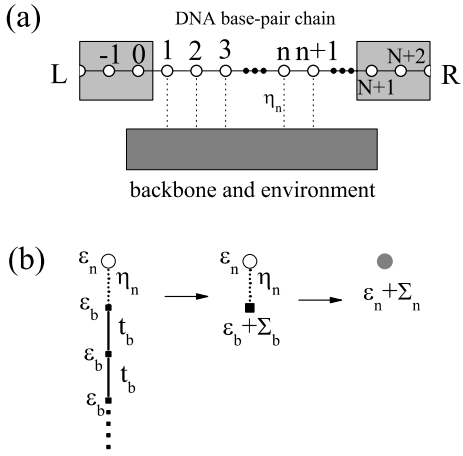

Fig. 5.2. a A schematic illustration of the one-dimensional chain model. The left and right ends of the DNA is connected to the electrode L and R and each site coupled to the dephasing reservoir of the backbone and the environment. **b** The dephasing reservoir for the site n is approximated as a semi-infinite chain and is renormalized as a self energy Σ_n

Any single-particle eigenstate can be expressed by the envelope wave function ψ_n in the site representation as $|\Psi\rangle = \sum_n \psi_n |n\rangle$ and the Schrödinger equation $\mathcal{H}_{\rm DNA}|\Psi\rangle = E|\Psi\rangle$ reads:

$$\begin{pmatrix} \varepsilon_1 - E & -t_{1,2} & \cdots & 0 & 0 & 0 & \cdots & 0 \\ -t_{1,2} & \varepsilon_2 - E & \cdots & 0 & 0 & 0 & \cdots & 0 \\ \cdots & \cdots & \cdots & \cdots & \cdots & \cdots & \cdots & \cdots \\ 0 & 0 & \cdots & \varepsilon_{n-1} - E & -t_{n-1,n} & 0 & \cdots & 0 \\ 0 & 0 & \cdots & -t_{n-1,n} & \varepsilon_n - E & -t_{n,n+1} & \cdots & 0 \\ 0 & 0 & \cdots & 0 & -t_{n,n+1} & \varepsilon_{n+1} - E & \cdots & 0 \\ \cdots & \cdots & \cdots & \cdots & \cdots & \cdots & \cdots & \cdots \\ 0 & 0 & \cdots & 0 & 0 & 0 & \cdots & \varepsilon_N - E \end{pmatrix} \begin{pmatrix} \psi_1 \\ \psi_2 \\ \cdots \\ \psi_{n-1} \\ \psi_n \\ \psi_{n+1} \\ \cdots \\ \psi_N \end{pmatrix} = 0 \,.$$

This is an equation group of N equations having the recursive form

$$-t_{n-1,n}\psi_{n-1} + (\varepsilon_n - E)\psi_n - t_{n,n+1}\psi_{n+1} = 0 \,, \tag{5.2}$$

and in principle, can be solved exactly for a closed system with a finite N. For a long homogeneous chain with $\varepsilon_n = \varepsilon$ and $t_{n,n+1} = t$, we have a periodic system and a Bloch type of wave function $\psi_n = \psi_0 \mathrm{e}^{\mathrm{i}kna}$ exists for the system. For the periodic boundary condition, i.e. $|N+n\rangle \equiv |n\rangle$ and $\psi_{N+n} \equiv \psi_n$, the energy $E = \varepsilon_n - t_{n-1,n}\psi_{n-1}/\psi_n - t_{n,n+1}\psi_{n+1}/\psi_n$ in (5.2) becomes

$$E = \varepsilon - 2t\cos(ka) \tag{5.3}$$

with $ka = \ell 2\pi/N$ for integer ℓ. This is an energy band centered at the on-site energy ε with a band width of four times the coupling parameter $4t$. The

Brillouin zone is $-\pi/a \leq k \leq \pi/a$ and the corresponding density of states (DOS) is $Na/(2\pi)(dk/dE) = N/[4\pi t \sin(ka)]$.

5.3.2 The Transfer Matrix Method

In an open system with a source of charge at one end of the DNA molecule and a drain at the other end (Fig. 5.2a), the system becomes infinitely large and the boundary condition for a closed system is no longer valid. The direct diagonalization of the Hamiltonian described above for the closed systems can not be used to find the transport properties. The transfer matrix method [40, 41] and the non-equilibrium Green's function theory [42] have been developed to solve the problem. The transfer matrix method is straightforward but it is not always the convenient choice for the complicated cases that involve taking into account many physical factors. In contrast, the Green's function theory appears more sophisticated for the simple cases but has the technical advantage when many physical factors are to be taken into account. Using simple examples like the homogeneous DNA chain, we can show that they are equivalent [23, 42]. In what follows, we have used the transfer matrix method.

One example of the open systems is a DNA duplex that is connected to a circuit via metal electrodes. Here the longitudinal charge migration from the source to the drain through the DNA duplex occurs when a voltage drop is applied between the electrodes. To facilitate the transport calculation in this system, the electrodes can be modelled as semi-infinite periodic one-dimensional tight-binding chain with uniform parameters of the on-site energy $\varepsilon_{\rm e}$, the band width of $4t_{\rm e}$, and the Fermi energy $\varepsilon_{\rm e}^{\rm F}$ measured from $\varepsilon_{\rm e}$. Furthermore, the contact properties between the DNA duplex and the left (right) electrode are described by the contact parameter $t_{\rm de}^{\rm L}$ ($t_{\rm de}^{\rm R}$). The total Hamiltonian then reads

$$\mathcal{H} = \sum_{n=-\infty}^{\infty} \varepsilon_n c_n^{\dagger} c_n - \sum_{n=-\infty}^{\infty} t_{n,n+1}(c_n^{\dagger} c_{n+1} + c_{n+1}^{\dagger} c_n)] \,. \tag{5.4}$$

Here the sites for $n \leq 0$ represent the left electrode and for $n \geq N+1$ the right electrode; $t_{0,1} = t_{\rm de}^{\rm L}$ and $t_{N,N+1} = t_{\rm de}^{\rm R}$ are the coupling parameters between the electrodes and the DNA chain.

The transport property of this open system is the electronic response of the drain (right) electrode to an injection of charge from the source (left) electrode. If the phase coherence length in the DNA is longer than the DNA length, we can assume a plane wave current injection and calculate the output plane wave function employing the recursion relation of the wave function in DNA (5.2). Rewriting (5.2) with the identity $\psi_n \equiv \psi_n$ in a recursion matrix form

$$\begin{pmatrix} \psi_{n+1} \\ \\ \psi_n \end{pmatrix} = \begin{pmatrix} \dfrac{\varepsilon_n - E}{t_{n,n+1}} & -\dfrac{t_{n-1,n}}{t_{n,n+1}} \\ 1 & 0 \end{pmatrix} \begin{pmatrix} \psi_n \\ \\ \psi_{n-1} \end{pmatrix} \,, \tag{5.5}$$

we obtain the above 2×2 transfer matrix $\hat{M}_n$ to derive the wave functions on sites $n+1$ and n from those on sites n and $n-1$. Note that (5.5) is a general form of the Schrödinger equation for any systems and the eigenstates of a closed system can be derived from it with proper boundary conditions. From (5.5), we can derive the wave function of the whole system once we know the wave functions of any two successive sites. For example, if we know the wave functions of sites 0 and -1 in the left electrode we can derive the wave functions of sites $N+1$ and N in the right electrode as

$$\begin{pmatrix} \psi_{N+1} \\ \psi_N \end{pmatrix} = \hat{M}_{\mathrm{T}} \begin{pmatrix} \psi_0 \\ \psi_{-1} \end{pmatrix} \tag{5.6}$$

with $\hat{M}_{\mathrm{T}} = \prod_{n=0}^{N+1} \hat{M}_n$ and evaluate the transmission of an electronic wave package from the left to the right electrode. Any propagating wave package can be expanded into a series of plane waves by the Fourier transform, and we can evaluate the transmission of the plane waves to get the overall transport properties. We consider that the hole wave functions in the source electrode has the general propagating form $\psi_n^{\mathrm{L}} = A\ \mathrm{e}^{\mathrm{i}k_{\mathrm{L}}na} + B\mathrm{e}^{-\mathrm{i}k_{\mathrm{L}}na}$ $(n \leq 0)$ with A being the incident wave amplitude and B the reflected wave amplitude, and in the drain electrode $\psi_n^{\mathrm{R}} = C\mathrm{e}^{\mathrm{i}k_{\mathrm{R}}na} + D\mathrm{e}^{-\mathrm{i}k_{\mathrm{R}}na}$ $(n \geq N+1)$ with C the transmitted wave amplitude. As the probability of carriers is proportional to the density of states, we choose the normalized incident amplitude $A = 1/\sqrt{|\sin(k_{\mathrm{L}}a)|}$. Here D represents the current injection from the right electrode and does not contribute to the current in this case. Nevertheless, we keep it here for the sake of generality of the formalism.

Substituting the wave function ψ_n^{L} and ψ_n^{R} into (5.6), we get

$$\hat{S}_{\mathrm{R}} \begin{pmatrix} D \\ C \end{pmatrix} = \hat{M}_{\mathrm{T}} \hat{S}_{\mathrm{L}} \begin{pmatrix} B \\ A \end{pmatrix} \tag{5.7}$$

with

$$\hat{S}_{\mathrm{L}} = \begin{pmatrix} 1 & 1 \\ \mathrm{e}^{\mathrm{i}k_{\mathrm{L}}a} & \mathrm{e}^{-\mathrm{i}k_{\mathrm{L}}a} \end{pmatrix} \tag{5.8}$$

and

$$\hat{S}_{\mathrm{R}} = \begin{pmatrix} \mathrm{e}^{-\mathrm{i}k_{\mathrm{R}}(N+2)a} & \mathrm{e}^{\mathrm{i}k_{\mathrm{R}}(N+2)a} \\ \mathrm{e}^{-\mathrm{i}k_{\mathrm{R}}(N+1)a} & \mathrm{e}^{\mathrm{i}k_{\mathrm{R}}(N+1)a} \end{pmatrix} . \tag{5.9}$$

We then have the transfer matrix for the amplitude $\hat{M}_{\mathrm{A}}$,

$$\begin{pmatrix} B \\ A \end{pmatrix} = \hat{M}_{\mathrm{A}} \begin{pmatrix} 0 \\ C \end{pmatrix}; \hat{M}_{\mathrm{A}} = \hat{S}_{\mathrm{L}}^{-1} \hat{M}_{\mathrm{T}}^{-1} \hat{S}_{\mathrm{R}} = \begin{pmatrix} M_{11} & M_{12} \\ M_{21} & M_{22} \end{pmatrix} . \tag{5.10}$$

Using $C = M_{22}^{-1} A$ and the group velocity $v = \mathrm{d}E/\mathrm{d}k = 2ta \sin ka$ for the tight-binding band, we arrive at the following expression for the transmission

$$T(E) = \frac{|C|^2}{|A|^2} \frac{v_{\mathrm{R}}}{v_{\mathrm{L}}} = \frac{|C|^2 \sin(k_{\mathrm{R}}a)}{|A|^2 \sin(k_{\mathrm{L}}a)} . \tag{5.11}$$

The conductance at an ideal transmission, i.e. 100%, through a quantum one-dimensional channel is the conductance quanta $e^2/h = (25.8\,\mathrm{k\Omega})^{-1}$ and in general, the current through the system is evaluated by the Landauer-Büttiker formula

$$I = \frac{2e}{h}\int_{-\infty}^{\infty} \mathrm{d}E\, T(E)[f(E-\mu_\mathrm{L}) - f(E-\mu_\mathrm{R})]\,. \tag{5.12}$$

Here, $f(E-\mu_\mathrm{X}) = 1/\exp[(E-\mu_\mathrm{X})/k_\mathrm{B}T_\mathrm{e}]$ is the Fermi function with the chemical potential μ_X of the electrode X for $X = \mathrm{L}$ or R and T_e is the environment temperature.

5.4 Charge Migration Through DNA

5.4.1 Charge Transfer Measurement

Both the chemical and physical techniques have been successfully used to measure the charge transfer rate in DNA. Usually, the conductance is measured indirectly in the chemical techniques such as the fluorescence quenching and the poly(G) trap methods. In the former case, a fluorescent molecule complex is inserted into the DNA and its fluorescence spectrum is measured after it is excited. The time-dependent fluorescent quenching is used to determine the transfer rate of the excited electrons in the fluorescent molecule [43]. In the latter case, a charge is injected into a single G base optically or electrically and the trapping rate at a double GG or a triple GGG trap is measured by water cleavage of the DNA strand [44]. In recent years, the conductance of DNA was also measured directly by physically connecting it to a circuit [3, 45, 46]. However, the conductance of the DNA extracted from different measurements appears to be very different [3, 45] and a consistent explanation of these results requires a systematic study and understanding of the mechanism of the charge transfer in different systems used in the experiments [47]. A reliable conclusion from any specific measurement depends on the understanding of the corresponding mechanism for the system in question, including the understanding of the charge transfer process in the DNA itself, the boundary condition or the contact effect, and participation of the environment.

5.4.2 Charge Transfer Via the DNA Molecule

In a long DNA complex, several mechanisms have been known to contribute to the charge transfer. Generally, we are considering a hole initially introduced to the DNA by the oxidation of a G base [43, 44]. Because the HOMO state of the G base has a lower ionization energy than the other bases, the G bases in DNA can work as charge stops and charge may hop back and forth from one G base to another during its long-distance migration [48–50]. In

a poly(G:C) DNA, an energy band forms in this periodic system and a charge can transport quickly through this band from one end to the other.

In DNA with a mixed (A:T) and (G:C) base pairs [51, 52], the (A:T) base pairs work as barriers for charges with energy of the G-base being the HOMO energy. A charge can tunnel from one G base to the next G base through the (A:T) barrier bridge between them. If the temperature is high enough, the charge can also gain thermal energy and oxidize the A bases so the charge can migrate through the DNA by thermal hopping. The role of the (A:T) bases in charge migration is a major focus of recent activities in the field.

Conventionally, a DNA is treated as a polymer chain of the base pairs when the charge transport is considered. Since the HOMO state in a (G:C) base pair is located at the G base and in an (A:T) base pair at the base A, charge is believed to migrate along a channel composed of the G and A bases. For the tunneling mechanism [53–57] the (A:T) base pairs located between the (G:C) base pairs are the tunneling potential barriers and the tunneling current should decay exponentially with the number of the (A:T) base pairs that are in the middle. For the thermal hopping mechanism [58–60], on the other hand, once an A base is oxidized with the help of the thermal energy, the other A bases can be easily oxidized. As a result, the hole can transport freely through the poly(A) channel and reach to the other end of the DNA without much resistance. In this case, the total resistance comes mainly from the first hop from the G base to an A base and the transfer rate is almost independent of the number of the (A:T) base pairs in the bridge.

In the above DNA chain model, each base pair is a unit. This picture is natural when discussing the entire electronic energy of the system stored in both inner and outer shell electronic states. The two paired bases in each base pair is strongly coupled with each other by the hydrogen bonds of the sigma orbits. In contrast, two stacked bases along the DNA chain are more weakly coupled by the overlap of the π orbits similar to the coupling between stacked graphene layers in a graphite. However, as far as the longitudinal charge transfer is concerned, the contribution of the σ orbits to the HOMO state and the participation of electrons in the σ orbits in the charge transfer process are negligible. This is due to the fact that the σ orbits have a much lower energy than that of the π orbits in the DNA bases. Accordingly, the charge transfer between the bases in a base pair is determined by the overlap of the π orbits between them. The *ab initio* calculations have shown that the overlap of the HOMO states between the two neighboring bases in the same strand is much stronger than that in different strands [25].

Based on the above considerations, the geometry of DNA (in a form of ladder network of the bases) may play an important role in the charge transfer and in some cases, it is more accurate to view a conducting DNA as two paired base strands rather than a chain of stacked base pairs. In that respect a DNA duplex is modelled as a ladder network [61–64] instead of a chain of HOMO

sites. When the geometry of the DNA molecule is taken into account, a charge can tunnel or thermally hop through different one-dimensional channels in the two-dimensional network.

5.4.3 Contact Effect

The contact property between the electrodes and the DNA duplex depends on the material of the electrode, the geometry of the contact, and the environment, and is by itself an active field of research in both physics and chemistry [65, 66]. How a DNA duplex makes contacts to the charge source or drain determines the efficiency of the charge injection and affects the measured results in the experiments. Unfortunately, in many cases, the details of the contact especially between the metal and DNA in direct transport measurements are not very clear. In the tight-binding model, an effective contact parameter is used to phenomenologically describe the contact. When a fixed voltage is applied between the source and the drain [30], the contact may significantly modify the potential profile across the DNA and the on-site energies vary accordingly. In the quantum tunneling-transport process, the charge injection efficiency is not a linear function of the contact parameter because of the phase interference. It has been shown that when a periodic DNA base chain with a uniform nearest-neighboring coupling parameter t is connected to a metal electrode of band width $4t_{\mathrm{e}}$, an optimal injection is achieved at $t_{\mathrm{de}} = \sqrt{t_{\mathrm{d}} \times t_{\mathrm{e}}}$ in the linear transport regime [22].

5.4.4 Dephasing Effect

It has been widely accepted that an electron in the HOMO state of a base in DNA can not only interact with the electrons in other bases but also with the background including the backbone and the environment, as illustrated by the dotted lines in Fig. 5.2a. The electron or the hole can jump out of the base to the background through the overlap of the outer-shell atomic orbits and through the electron-phonon interaction (coupling with the inner-shell atomic orbits and the nuclear states). As a simple approximation, the effect of the background on site n can be integrated into a self energy $\Sigma_n = \Sigma_n^{\mathrm{R}} + \mathrm{i}\Sigma_n^{\mathrm{I}}$, in which the real part offers the energy correction to the on-site energy and the imaginary part to the dephasing effect. Just as for the electrodes, we can model the background as a semi-infinite one-dimensional tight-binding chain as depicted schematically in Fig. 5.2b. The effective Hamiltonian for the coupling between the site n and the background reservoir can be simplified as a 2×2 matrix for a two-level system [42]

$$\hat{\mathcal{H}}_n^{\mathrm{dph}} = \begin{pmatrix} \varepsilon_n & -\eta_n \\ -\eta_n & \varepsilon_{\mathrm{b}} + \Sigma_{\mathrm{b}} \end{pmatrix} , \tag{5.13}$$

where η_n is the coupling parameter between the site n and the background, ε_{b} is the on-site energy of the first site in the semi-infinite chain of the background, and the self energy Σ_{b} represents the effect from the other sites of

the dephasing chain. We have to keep in mind that here again we are concerned with the response of the system to a wave package of any energy E rather than the eigenstates of a closed system and the Schrödinger equation $\mathcal{H}_n^{\rm dph}|\varphi\rangle = E|\varphi\rangle$ requires $(\varepsilon_n - E)(\varepsilon_{\rm b} - \Sigma_{\rm b} - E) = \eta_n^2$. The self energy on the site n in the DNA chain due to the dephasing reservoir, $\Sigma_n = E - \varepsilon_n$, for a carrier of energy E then reads

$$\Sigma_n = \frac{\eta_n^2}{(E - \varepsilon_{\rm b} - \Sigma_{\rm b})} \,. \tag{5.14}$$

Similarly, $\Sigma_{\rm b}$ can be obtained self consistently using this expression by replacing Σ_n with $\Sigma_{\rm b}$ and η_n with $t_{\rm b}$, the nearest neighbor coupling parameter for the dephasing chain. We have $\Sigma_{\rm b} = (E-\varepsilon_{\rm b})/2+{\rm i}[t_{\rm b}^2-(E-\varepsilon_{\rm b})^2/4]^{1/2}$ [67,68].

5.5 Understanding the Weak Distance Dependence

The possibility of charge transfer in DNA has been proposed soon after the atomistic DNA structure was established [8, 9]. However, quantitatively the distance dependence of charge transfer in DNA was measured systematically only several decades later [69]. It has been well established that the charge can transfer from the donor to the acceptor through the intermediate bridges (molecular clusters) of higher energy via the electronic superexchange interaction along a molecular chain. In this picture, the bridges work as a tunneling barrier and the donor and acceptor are treated as charge traps. With the help of the electron-phonon (vibronic) interaction, the tunneling can occur when the donor and the acceptor states are not degenerate. A perturbation theory based on the tight-binding model has been developed to describe this charge transfer mechanism as early as the first proposal of charge transfer in DNA [53]. Exponential decay of the transfer rate with the distance was predicted. This strong exponential distance dependence in the molecular chain has been confirmed by many experiments and also by different theoretical formalisms in the years that followed. However, many measurements have also shown a weak distance dependence of charge transfer in the DNA [43, 44, 69–72]. This means that charges may transfer along a very long distance and indicate the possible importance of the thermally-induced hopping between the G and G's bases [58–60]. In order to clearly identify the regimes for the validity of the different mechanisms, Giese et al., carried out a systematic measurement of the charge transfer between the (G:C) and $(G:C)_3$ charge traps over $(T:A)_{\mathcal{M}}$ bridges of higher energy [44]. That experiment demonstrated an exponential decay rate versus the distance for $\mathcal{M} \leq 3$ and an almost flat distance dependence for $\mathcal{M} > 3$ with a crossover around $\mathcal{M}_{\rm c} = 3$ as shown in Fig. 5.3.

Naturally, this flat distance dependence was connected qualitatively to the thermally-induced hopping mechanism. Based on this proposal, many

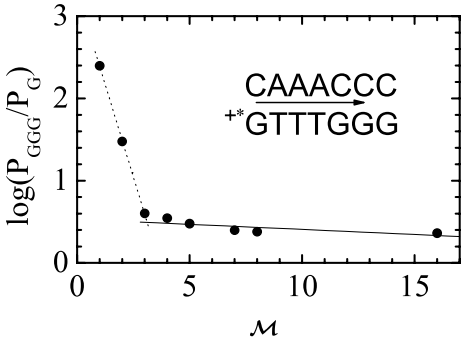

Fig. 5.3. Logarithm of the efficiency of the charge transfer (*filled circles*), measured by the ratios of the irradiation products P_{GGG}/P_G in [44], from the (G:C) to triple (G:C) base pairs, plotted as a function of the number $\mathcal{M}$ of (A:T) base pairs in a (G:C)(A:T) $_{\mathcal{M}}$(G:C)$_3$ DNA duplex. The linear fit to the results for $1 \leq \mathcal{M} \leq 3$ is $\log(P_{GGG}/P_G) = 3.3–0.9\mathcal{M}$ as shown by the *dotted line* and for $4 \leq \mathcal{M} \leq 16$ is $\log(P_{GGG}/P_G) = 0.5–0.01\mathcal{M}$ as shown by the *solid line*

authors have contributed to a quantitative explanation of the experimental result. Berlin, Burin, and Ratner [37] used a tight-binding (Hückel) model for a one-dimensional chain with each base pair as a site and derived the crossover number when the tunneling transfer rate is equal to the transfer rate by the activation process to the (T:A) tight-binding band. For a barrier height of 0.46 eV (between the site energies of (G:C) and (T:A) or (A:T) base pairs) and the coupling parameter in the range from 0.1 eV to 0.4 eV, the crossover number is found to lie between 3 and 4, in agreement with the experiment. Bixon and Jortner [73, 74] emphasized the difference between the intra- and interstrand couplings for different base sequences and proposed that the charge transfer occurs along a dominant path. They applied the kinetic-quantum mechanical model for the thermally-induced hopping process and fitted the experimental result. However, they noticed some inconsistency in the theory and concluded that the theory does not explain the result. Renger and Marcus [75] proposed that the flat distance dependence can be explained by integrating the variable-range hopping concept into the kinetic model. In addition, describing the system with the Su-Schrieffer-Heeger model and the Hubbard Hamiltonian, Cramer, Krapf, and Koslowski [76] obtained the energy potential surface in the atomistic level for evaluation of the transfer rate based on the Marcus theory. They also explained the crossover from the exponential to the flat distance dependence in the picture of tunneling and thermal hopping transition. Basko and Conwell [77] emphasized the importance of phonons in the process and proposed that the formation of polarons [78–82] in the system is key for the flat distance dependence.

It is known [39] that the quantum interference can play an important role in a system with multi-tunneling channels and a resistance ladder network has

very different properties than a series of resistance. In this work, we explore the transport properties of a DNA duplex that is treated as a tunneling ladder network [83].

5.6 Electron Tunneling Through Multi-Path Barriers

5.6.1 The Double-Stranded Model

In order to take into account the duplex geometry of the primary structure, we consider a DNA duplex chain of N Watson-Crick base pairs connected to four semi-infinite one-dimensional electrodes with one for each end of the first and the second strand as illustrated in Fig. 5.4. The four electrodes are assumed independent of each other since in many cases the charges are injected into one base and trapped in another bases at the ends. The tight-binding Hamiltonian of the system is

$$\begin{aligned}\mathcal{H} = &\sum_{n=-\infty}^{\infty} [\varepsilon_n c_n^\dagger c_n - t_{n,n+1}(c_n^\dagger c_{n+1} + c_{n+1}^\dagger c_n)] \\ &+ \sum_{n=-\infty}^{\infty} [u_n d_n^\dagger d_n - h_{n,n+1}(d_n^\dagger d_{n+1} + d_{n+1}^\dagger d_n)] \\ &- \sum_{n=1}^{N} \lambda_n (c_n^\dagger d_n + d_n^\dagger c_n) \, .\end{aligned}$$

Here $c_n^\dagger$ ($d_n^\dagger$) is the creation operator of holes in the first (second) strand on site n of the DNA chain (for $1 \le n \le N$), the left electrodes ($n \le 0$), and the right electrodes ($n \ge N+1$). The coupling parameter of the first (second) strand $t_{n,n+1}$ ($h_{n,n+1}$) is equal to the intra-strand coupling parameter t_{d}

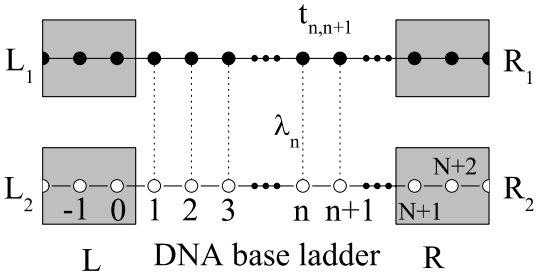

Fig. 5.4. Schematic illustration of the two-stranded model. The first strand (*filled circle*) has a DNA base sequence G(T)$_{\mathcal{M}}$GGG and the second strand (*empty circle*) a sequence C(A)$_{\mathcal{M}}$CCC. The four *gray areas* indicate the four virtual electrodes connected to the DNA chain. Current is injected into the first strand through the left electrode L_1 and measured at the right electrode R_1

between neighboring sites n and $n+1$ of the DNA for $1 \leq n \leq N-1$, one-fourth of the conduction band-width in the electrodes t_{e} for $n \leq -1$ and $n \geq N+1$, and the coupling strength t_{de} between the electrodes and the DNA strands for $n = 0$ and $n = N$. The inter-strand coupling between the sites in the same Watson-Crick base pair is described by λ_n.

In the site representation, the Schrödinger equation is an equation group with two inequivalent form of equations

$$\begin{aligned} t_{n-1,n}\psi_{n-1} + (E - \varepsilon_n)\psi_n + \lambda_n\phi_n + t_{n,n+1}\psi_{n+1} = 0 \\ h_{n-1,n}\phi_{n-1} + (E - u_n)\phi_n + \lambda_n\psi_n + h_{n,n+1}\phi_{n+1} = 0 \,, \end{aligned}$$

where ψ_n (ϕ_n) is the wave function of the first (second) strand on site n. The wave functions of the sites $n+1$ and n are related to those of the sites n and $n-1$ by a 4×4 transfer matrix $\hat{M}_n$,

$$\begin{pmatrix} \psi_{n+1} \\ \phi_{n+1} \\ \psi_n \\ \phi_n \end{pmatrix} = \hat{M}_n \begin{pmatrix} \psi_n \\ \phi_n \\ \psi_{n-1} \\ \phi_{n-1} \end{pmatrix} \,, \tag{5.15}$$

with

$$\hat{M}_n = \begin{bmatrix} \dfrac{(\varepsilon_n - E)}{t_{n,n+1}} & \dfrac{-\lambda_n}{t_{n,n+1}} & -\dfrac{t_{n-1,n}}{t_{n,n+1}} & 0 \\ \dfrac{-\lambda_n}{h_{n,n+1}} & \dfrac{(\varepsilon_n - E)}{h_{n,n+1}} & 0 & -\dfrac{h_{n-1,n}}{h_{n,n+1}} \\ 1 & 0 & 0 & 0 \\ 0 & 1 & 0 & 0 \end{bmatrix} \,.$$

Assuming the plane wave injection and transmission in the electrodes and following the same process as described in (5.6)–(5.12) for the one-dimensional chain model, we can evaluate the charge transfer rate to any electrode from one injection electrode in the double-stranded model.

5.6.2 Charge Transfer Through a (G:C)(T:A)$_{\mathcal{M}}$(G:C)$_3$ DNA

We now apply the double-stranded model to describe the intra-molecular hole transfer along the DNA duplex chain (G:C)(T:A)$_{\mathcal{M}}$(G:C)$_3$ measured by Giese et al. and described in Sect. 5.5. To minimize the contact effect introduced by the virtual electrodes we introduced to facilitate the calculation, we assume a strong coupling (of coupling parameter $t_{0,1} = t_{N,N+1} = h_{0,1} = h_{N,N+1} = t_{\mathrm{de}} \geq 1.5\,\mathrm{eV}$) between the electrodes and the sites at the ends of the DNA strands, and choose a band width ($4t_{\mathrm{e}}$) in the electrodes such that the optimal injection condition $t_{\mathrm{d}} \times t_{\mathrm{e}} = t_{\mathrm{de}}^2$ [22] is satisfied. The result is found to be independent of the choice of the value of t_{de} once it is much larger than the coupling parameter between the sites inside the DNA. In this case,

the added electrodes do not become a bottleneck of the system for the charge transfer and the calculated result predominantly reflects the properties of the DNA duplex.

To evaluate the transfer rate or current of a charge (hole) from the donor at the left-end site to the acceptor at the right-end site of the first strand, we need to know the chemical potential at each end. In the experiment of [44], a hole was injected to the left-end site. This means that the left chemical potential is approximately the on-site energy of this site while the right one is less. During the charge transfer process, the hole may retain the same energy if no inelastic scattering occurs or loose energy via the electron-phonon scattering or other inelastic collisions [17]. Real electron-phonon scattering at the donor and acceptor contributes to the reorganization energy and affects the temperature dependence of charge transfer [11, 36, 84] while the virtual electron-phonon interaction may affect the electronic coupling between different sites [85]. In the case of strong electron-phonon coupling, the charge may be dressed by the phonon cloud and transforms into a quasiparticle, the polaron [78, 79]. Here we assume that the virtual phonon effect and the polaron effect can be simplified as an adjustable to the coupling parameter between sites. Since we are concerned with distance dependence of the transfer, we do not deal with the inelastic scattering mechanisms at the donor and the acceptor sites explicitly but analyze two limiting situations, between which the real charge transfer process would occur. Since our results for the distance dependence of the transfer rate from the two limits converge (see below), we conclude that our results are reliable.

In the first limit, we assume that there is no inelastic scattering involved and the hole energy is conserved during the transfer process. The transfer rate is proportional to the conductance of the system at equilibrium. For a small electric potential difference $k_{\mathrm{B}}T_{\mathrm{e}}/\,\mathrm{e}$, the current is

$$I = \frac{2\,\mathrm{e}}{h}\int_{-\infty}^{\infty} \mathrm{d}E\, T(E)[1 - f(E-\mu)]f(E-\mu)\,, \tag{5.16}$$

with μ equal to the on-site energy of site 1 in the first strand and $T_{\mathrm{e}} = 300\,\mathrm{K}$.

In the second limit, we assume that the hole can lose energy freely during the charge transfer process before or after the tunneling, and the transfer rate is proportional to the total current via all channels of energies below the hole's initial energy. This corresponds to an infinitely low chemical potential at the right electrode and the current is

$$I = \frac{2e}{h}\int_{-\infty}^{\infty} \mathrm{d}E T(E) f(E-\mu)\,. \tag{5.17}$$

We now calculate the distance dependence of the transfer rate using (5.16) and (5.17) in a DNA duplex, where the first strand has the base sequence $\mathrm{G(T)}_{\mathcal{M}}\mathrm{GGG}$ as in the experiment of [44]. For the sake of simplicity and to focus on the geometry effect, a uniform intra-strand hopping parameter

$t_{n,n+1} = h_{n,n+1} = t_{\rm d}$ $(1 \le n \le N-1)$ and a uniform inter-strand hopping parameter $\lambda_n = \lambda_{\rm d}$ $(1 \le n \le N)$ between any two neighboring bases in the DNA are used.

First we switch off the inter-strand coupling and calculate the dependence of the current I on $\mathcal{M}$ as shown in Fig. 5.5a, for different values of the intra-strand coupling parameter $t_{\rm d}$. We find an exponential dependence of the current

$$I = I^{\mathcal{M}} \propto {\rm e}^{-\beta \mathcal{M} a} \tag{5.18}$$

when $t_{\rm d}$ is much smaller than the bridge barrier height $E_{\rm T} - E_{\rm G}$. We then extract the values of β for different $t_{\rm d}$ and plot in Fig. 5.5c as β versus $\ln(t_{\rm d})$ calculated via (5.17). The curves are almost linear, very similar to the results of (5.16), and converge to the approximate formula

$$\beta = \frac{2}{a} \left| \ln \frac{t_{\rm d}}{E_{\rm T} - E_{\rm G}} \right| \ . \tag{5.19}$$

This is the well-known one-dimensional superexchange result in the literature and has been derived in many different ways [37, 39, 53, 73].

In the next step, we fix $t_{\rm d}$ and switch on the inter-strand coupling by varying $\lambda_{\rm d}$. The result is displayed in Fig. 5.5b where we choose $t_{\rm d} = 0.5\,{\rm eV}$ and plot I versus $\mathcal{M}$ for a series of $\lambda_{\rm d}$. Note that the charge transfer occurs via π-electrons and generally $\lambda_{\rm d} < t_{\rm d}$ [25]. For finite $\lambda_{\rm d}$, the current drops

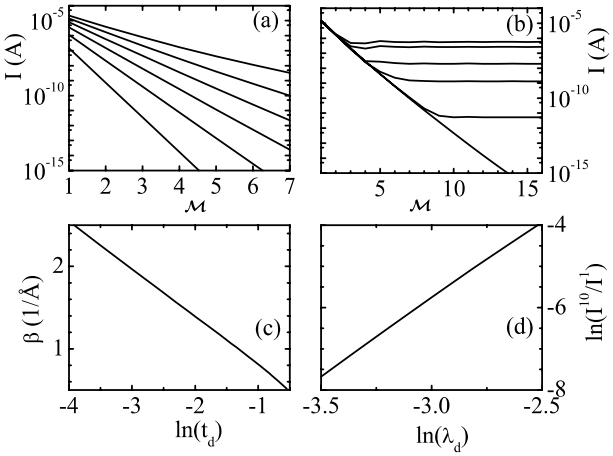

Fig. 5.5. **a** Current I versus $\mathcal{M}$ for $t_{\rm d} = 0.1, 0.2, 0.3, 0.4, 0.5, 0.6\,{\rm eV}$ (from *lower* to *upper curves*) for zero inter-strand coupling. The displayed results are from (5.17) and identical results are obtained from (5.16) in all the *panels*. **b** Same as in **a** at fixed $t_{\rm d} = 0.5\,{\rm eV}$ but for $\lambda_{\rm d} = 0, 5, 20, 40, 80, 100\,{\rm meV}$ corresponding to curves counted from the *bottom*. **c** The β value calculated from the slope of the lines in **a** versus $\ln t_{\rm d}$. **d** $\ln(I^{10}/I^1)$, where $I^{\mathcal{M}}$ is the current for a chain with $\mathcal{M}$ (A:T) base pairs, versus $\ln \lambda_{\rm d}$. The unit of $t_{\rm d}$ and $\lambda_{\rm d}$ is eV and $t_{\rm de} = 1.5\,{\rm eV}$ [83]

exponentially with increasing $\mathcal{M}$ for small $\mathcal{M}$ and then becomes almost flat with oscillations around a limiting current I^{∞} for large $\mathcal{M}$. The crossover number $\mathcal{M}_{\rm c}$ depends on the strength of the inter-strand coupling parameter. The weaker the inter-strand coupling is, the bigger the $\mathcal{M}_{\rm c}$. The dependence of I^{∞} on $\lambda_{\rm d}$ is approximately illustrated in Fig. 5.5d, where the normalized current I^{10}/I^{1} of the DNA chain at $\mathcal{M} = 10$ is plotted versus $\ln(\lambda_{\rm d})$. Again, two almost identical straight lines are found corresponding to the two limiting situations based on (5.16) and (5.17) and can be approximately expressed as

$$\ln(I^{10}/I^{1}) = 5.7 + 3.9\ln(\lambda_{\rm d})\ . \tag{5.20}$$

From (5.18)–(5.20), we estimate the ratio of inter- and intra-strand coupling from the crossover number $\mathcal{M}_{\rm c}$. Since the environment can change $\lambda_{\rm d}/t_{\rm d}$, we predict that the transition number may vary and be different from 3 when the experimental environment changes.

Calculating the current I before and after adding a (T:A) base pair at site n with zero or nonzero inter-strand coupling λ_n, we find that the distance-dependence crossover has a topological origin, e.g., from the one-dimensional chain charge transport to a partly two-dimensional ladder network. When a new (T:A) base pair is inserted into the DNA chain, a new superexchange channel is opened through its inter-strand coupling and the corresponding contribution compensates the loss of charge transfer rate that would incur because of an extra barrier to the existing channels [83].

In Fig. 5.6, we fit the $\mathcal{M}$ dependence of the charge transfer rate observed in [44] using intra- and inter-strand coupling parameters $t_{\rm d} = 0.52\,{\rm eV}$ and $\lambda_{\rm d} = 0.07\,{\rm eV}$ respectively. (5.17) is employed in the calculation. The agree-

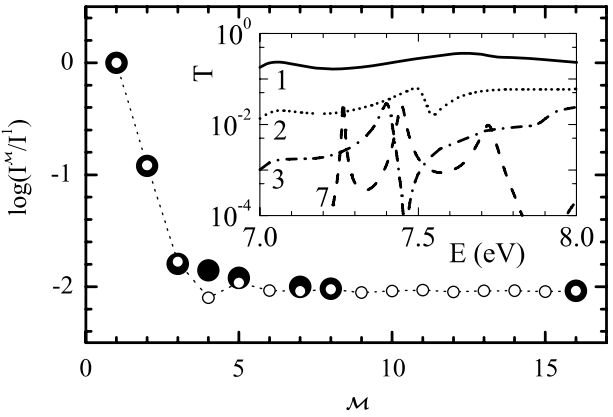

Fig. 5.6. Normalized transfer rate measured in [44] (*filled circle*) and theoretical fit using this model (*open circle*), $\log(I^{\mathcal{M}}/I^{1})$, are plotted as functions of $\mathcal{M}$ (T:A) base pairs between the (G:C) and the triple (G:C) base pairs. *Inset*: The corresponding transmission T versus energy E for $\mathcal{M} = 1$ (*solid line*), 2 (*dotted line*), 3 (*dot-dashed line*), and 7 (*dashed line*). Here $t_{\rm de} = 3\,{\rm eV}$ is used [83]

ment between the experimental and theoretical results are very good except for a small oscillation in the theoretical result near $\mathcal{M}_c$. This oscillation results in the deviation of the empty circle from the filled circle at $\mathcal{M} = 4$. When (5.16) is used, similar result is obtained but with a stronger oscillation. The oscillations reflect the fact that we have treated the system as a coherent system by neglecting the dephasing effect from the environment and the relaxation process from phonons.

To get a clear picture of the process, we plot as inset in Fig. 5.6, the transmission T as a function of the hole energy E for systems with $\mathcal{M} = 1, 2, 3$, and 7 in an energy range near and below the G base HOMO energy E_G. In the T spectrum, each peak represents a transport channel and there are more fine structures or peaks when more base pairs are added to the system. When $\mathcal{M}$ varies from 1 to 3, the one-dimensional chain transport dominates and only one principal transmission peak is important. The principal peak shifts when $\mathcal{M}$ varies due to the shift of energy of the channel; its height drops rapidly leading to an exponential decrease of charge transfer rate. If we add more (T:A) base pairs to the DNA duplex, the principal T peak drops to a level comparable to that of other peaks and results in a crossover from the one-dimensional chain transport to a two-dimensional network transport. In the absence of any inelastic scattering the charge transfer rate versus $\mathcal{M}$ oscillates as a result of the energy shift of the transport channels and the energy conservation of the charge. With the assistance of the phonon, however, the charge can use channels of energy different from its initial energy and phonons may play an important role in assisting the charge transfer.

In the above analysis, we also neglect the dephasing effect and the interstrand coupling between two neighbor base pairs. The dephasing effect exists in a real system and can help damp the oscillation of the current observed in Figs. 5.5 and 5.6. It has been shown by the *ab initio* calculation that the interstrand coupling between two nearest neighbor base pairs is also important. This coupling can be easily integrated into the transfer matrix by adding non-zero elements. This coupling has similar effects on charge tunneling as λ_n and similar curves as in Fig. 5.5b are obtained if replace λ_n by it.

5.7 Transverse Tunneling Current

In this section, we provide a detailed review of charge transport in single-stranded DNA in the direction *perpendicular* to the backbone axis [6, 86]. As pointed out in [4], this approach might be useful in providing a low-cost, but rapid DNA sequencing. We also discuss the conditions for formation of bipolarons in DNA, and possible experimental manifestation of bipolarons in transverse tunneling experiments.

5.7.1 Rate Equation

The longitudinal transport along the DNA molecule is determined by the properties of the whole DNA, which consists of many basic elements, viz.

the base pairs. In this sense longitudinal charge transfer is the tool to probe the properties of the whole molecule. In what follows, we address another problem, namely, how to study the local properties of the DNA molecule. We discuss here the method to extract the local energy characteristics of the molecule. The only way to measure the local characteristics of an extended DNA molecule is to study the transport in the direction perpendicular to the backbone axis, i.e. the transverse tunneling current [6, 86]. Since the most important local parameters of DNA are the characteristics of electron and hole traps, below we consider only transverse tunneling through electron or hole DNA traps. In this case, if the electrodes have a relatively small width, the tunneling occurs through a single DNA base pair. The linear (unstructured) tunneling conductance then depends on the particular type of base pair [6]. This fact can be used to discover the sequence of DNA by scanning it with conducting probes. We demonstrate below that not only the linear conductance of the tunneling current but also the *structure* of the I–V curves can provide important information on the properties of the DNA, in particular, about the trapping spots. This is because the tunneling current through the system is determined by its density of states (DOS). For a finite system, the DOS has peaks corresponding to discrete energy levels. These peaks will result in a staircase structure of the tunneling current as a function of the applied voltage whenever the Fermi levels align with a new state of the system and thereby open an additional channel for tunneling. Therefore, from the staircase structure of the I–V curve one can learn about the energy spectra of the system. For DNA the trapping spots consist of a finite number of base pairs. Hopping between the base pairs within the traps determines the energy spectra of the spots. In addition to the energy scale due to hopping, there is also an energy scale due to the hole-phonon (or electron-phonon) interaction. Finally, for DNA trapping spots, the I–V dependence has two types of staircase structure; one due to the hopping and the other due to the phonons.

The tunneling transport through a single molecule or a quantum dot with electron-phonon coupling has been extensively studied in the literature [87–90]. The main outcome of these works is the staircase structure of the I–V curves due to the phonon sidebands. The heights of the steps in this structure depend on the strength of the electron-phonon interactions, temperature, and on the equilibrium condition of the electron-phonon system. These studies were mainly restricted to a molecule with a single-electron energy level, although a general approach to a many-level system is also formulated [89]. The DNA trap can be considered as a system of a few molecules (base pairs) with the hopping between them and the electron-phonon coupling. Below, we consider only the hole traps and the tunneling current of holes, but the analysis is also valid for electron traps and electron transport. Whether it is a hole transport or electron transport depends on the gate potential, i.e. on the position of the chemical potential at the zero source-drain voltage V_{sd}.

At first, we study a single-hole transport through the DNA molecule and disregard the effects related to the Coulomb blockade [91] or to a double occupancy of the DNA traps, assuming that the repulsion between the holes is strong enough. In the next section we will analyze the possibility for formation of a bound state of two holes in a trap due to the bipolaronic effect and discuss the manifestation of such a bound state in the transverse tunneling transport.

For a single hole in the trap, the Hamiltonian of the DNA trap and the electrodes consists of three parts: (i) the DNA trap Hamiltonian which includes the tight-binding hole part with hopping between the nearest base pairs (one-dimensional chain model discussed in Section 5.2.1) and the Holstein's phonon Hamiltonian with diagonal hole-phonon interaction [78], (ii) the Hamiltonian of the two leads, left (L) and right (R), and (iii) the Hamiltonian corresponding to the tunneling between the leads and DNA traps

$$\mathcal{H} = \mathcal{H}_{\rm trap} + \mathcal{H}_{\rm leads} + \mathcal{H}_{\rm t} \ , \tag{5.21}$$

with

$$\begin{aligned} \mathcal{H}_{\rm trap} = & \sum_{n=1}^{N_{\rm t}} \varepsilon \, c_n^\dagger c_n - t \sum_i \left[c_n^\dagger c_{n+1} + h.c. \right] + \\ & + \hbar\omega \sum_n b_i^\dagger b_n + \chi \sum_n c_n^\dagger c_n \left(b_n^\dagger + b_n \right) , \end{aligned} \tag{5.22}$$

$$\mathcal{H}_{\rm leads} = \sum_{k,\alpha={\rm L,R}} \varepsilon_k \, d_{\alpha,k}^\dagger d_{\alpha,k}, \tag{5.23}$$

$$\mathcal{H}_{\rm t} = -t_0 \sum_{\alpha={\rm L,R},k} \left[c_{n_0}^\dagger d_{\alpha,k} + h.c. \right] \ , \tag{5.24}$$

where c_i is the annihilation operator of the hole on site (base pair) n, ε is the on-site energy of the hole in the trap (same for all base pairs within the trap and is determined by the gate voltage or doping of DNA), b_i is the annihilation operator of a phonon on site i, t is the hopping integral between the nearest base pairs, ω is the phonon frequency, χ is the hole-phonon coupling constant, and $d_{\alpha,k}$ is the annihilation operator of a hole in the lead $\alpha = {\rm L, R}$ with momentum k. The index $n = 1, \ldots, N_{\rm t}$ in (5.22) labels the sites (base pairs) in the trap and $N_{\rm t}$ is their total number. Tunneling from the leads to the trap occurs only to the site n_0 with the tunneling amplitude t_0. In the hole-phonon part of the DNA Hamiltonian $\mathcal{H}_{\rm trap}$, we include only the optical phonons [92] with diagonal hole-phonon interaction.

We describe the process of tunneling through the trap as a sequential tunneling [93]. In the weak lead-trap coupling regime, the tunneling Hamiltonian $\mathcal{H}_{\rm t}$ can be considered as a perturbation which introduces the transitions between the states of the trap Hamiltonian, $\mathcal{H}_{\rm trap}$. We denote the eigenstates of the trap Hamiltonian without coupling to the leads as $|0, m\rangle$ with energy $E_{0,m}$ for the trap without any holes, and $|1, p\rangle$ with the energy $E_{1,p}$ for a trap

with a single hole. In the weak lead-trap coupling limit, the master equation for the density matrix of the trap reduces to the rate equation [88] for probability $P_{0,m}$ to occupy the state $|0,m\rangle$ and probability $P_{1,p}$ to occupy the state $|1,p\rangle$,

$$\frac{dP_{1,p}}{dt} = \sum_{m,\alpha=\mathrm{L,R}} W^{0\to1}_{\alpha,mp} P_{0,m} - \sum_{m,\alpha=\mathrm{L,R}} W^{1\to0}_{\alpha,pm} P_{1,p} - \\ - \frac{1}{\tau}\left[P_{1,p} - P^{\mathrm{eq}}_{1,p} \sum_{n'} P_{1,p'}\right], \tag{5.25}$$

$$\frac{dP_{0,m}}{dt} = \sum_{n,\alpha=\mathrm{L,R}} W^{1\to0}_{\alpha,pm} P_{1,p} - \sum_{n,\alpha=\mathrm{L,R}} W^{0\to1}_{\alpha,mp} P_{0,m} - \\ - \frac{1}{\tau}\left[P_{0,m} - P^{\mathrm{eq}}_{0,m} \sum_{m'} P_{0,m'}\right]. \tag{5.26}$$

In the above equations the distributions $P^{\mathrm{eq}}_{1,p}$ and $P^{\mathrm{eq}}_{0,m}$ are the corresponding equilibrium distributions with temperature T,

$$P^{\mathrm{eq}}_{1,p} = \exp\left(-E_{1,p}/kT\right) / \sum_{p'} \exp\left(-E_{1,p'}/kT\right)$$

and

$$P^{\mathrm{eq}}_{0,m} = \exp\left(-E_{0,m}/kT\right) / \sum_{m'} \exp\left(-E_{0,m'}/kT\right) .$$

Here τ is the relaxation time which is assumed to be the same with or without a hole in the trap. The transition rate $W^{1\to0}_{\alpha,pm}$ is the rate of hole tunneling from the state $|1,p\rangle$ of the trap to the $\alpha = \mathrm{L,R}$ lead leaving the trap in the state $|0,m\rangle$. Similarly, the rate $W^{0\to1}_{\alpha,mp}$ is the rate of hole tunneling from the lead α to the state $|1,p\rangle$ of the trap, while originally the trap was in the state $|0,m\rangle$. These rates can be found from Fermi's golden rule

$$W^{1\to0}_{\alpha,pm} = \Gamma_0 f_\alpha\left(E_{1,p} - E_{0,m}\right) \left|\langle 0,m|\, c_{n_0}\, |1,p\rangle\right|^2, \tag{5.27}$$

$$W^{0\to1}_{\alpha,mp} = \Gamma_0 \left[1 - f_\alpha\left(E_{1,p} - E_{0,m}\right)\right] \left|\langle 0,m|\, c_{n_0}\, |1,p\rangle\right|^2 , \tag{5.28}$$

where $\Gamma_0 = 2\pi t_0 \rho/\hbar$ and ρ is the density of states in the leads, which is assumed to be the same in "L" and "R" leads, and $f_\alpha(\epsilon)$ is the Fermi distribution function of the lead α with a chemical potential μ_α. The rate equations (5.25)–(5.26) also assume that the temperature is high enough, i.e. $kT \gg \Gamma$. This means that during the tunneling, the hole state loses its coherence, so the system can be characterized only by the diagonal elements of the density matrix, i.e. by the probabilities to occupy the states in the trap.

For the stationary case, the time derivatives of $P_{1,p}$ and $P_{0,m}$ are zero and (5.25)–(5.26) become a system of linear equations with the normalization

condition $\sum_p P_{1,p} + \sum_m P_{0,m} = 1$. The corresponding stationary current can be calculated as

$$I = \sum_{p,m} \left[P_{0,m} W^{0\to 1}_{\mathrm{L},mp} - P_{1,p} W^{1\to 0}_{\mathrm{L},pm} \right] . \tag{5.29}$$

The procedure of finding the I–V dependence is the following: At first we calculate the energy spectra and wave functions of the hole-phonon trap system. Then at a given bias and the gate voltages, we calculate the tunneling rates (5.27)–(5.28). As a last step, we solve the linear system of equations (5.25)–(5.26) to find the probabilities $P_{0,m}$ and $P_{1,p}$ and the tunneling current (5.29).

5.7.2 Single-Particle Tunneling

There are few general remarks we can make in relation to the system of equations (5.25)–(5.29). Since the tunneling occurs only through a single base pair, the I–V characteristics should also depend on the position of the base pair through which the tunneling current is measured. This dependence can be illustrated for the hole system without the hole-phonon interactions. For such a system we have only the hopping of the hole within the finite trap system with a finite number of sites (base pairs). The corresponding hopping Hamiltonian of the trap takes the form

$$\mathcal{H}_{\mathrm{trap}} = \sum_{n=1}^{N_{\mathrm{t}}} \varepsilon\, c_n^{\dagger} c_n - t \sum_i \left[c_n^{\dagger} c_{n+1} + h.c. \right] . \tag{5.30}$$

Assuming zero boundary conditions at the ends of the trap, i.e. deep trap approximation, we can easily find the hole wave functions within the trap as

$$\Psi_K(n) = \sin\left(\frac{\pi K}{N_{\mathrm{t}+1}} n \right) , \tag{5.31}$$

where $K = 1, \ldots, N_{\mathrm{t}}$. It is easy to check that the functions $\Psi_K(n)$ satisfy the boundary conditions $\Psi_K(n = 0) = \Psi_K(n = N_{\mathrm{t}+1}) = 0$. The energy corresponding to the state Ψ_K is $\epsilon_K = -2t \cos(\pi K/(N_{\mathrm{t}+1}))$. Therefore, for a finite trap with N_{t} sites there are N_{t} energy levels within the trap. Generally, if we measure the transverse tunneling current then we should expect N_{t} steps in the I–V dependence, where each step corresponds to a single energy level. This is not the case when the tunneling occurs through a single base pair because then the contribution to the tunneling current of the Kth state will be proportional to $\sin^2(\pi K n_0/(N_{\mathrm{t}+1}))$. If this coefficient is zero then there is no contribution of the corresponding state and the step related to this state will be suppressed. For example, for $N_{\mathrm{t}} = 2$ and 4 and for any positions of the tunneling site, n_0, there are always N_{t} steps in the I–V dependence. A more interesting structure is expected for $N_{\mathrm{t}} = 3$ and 5. It is easy to see that for

$N_t = 3$ there are three steps for $n_0 = 1$ and two steps for $n_0 = 2$ since in the last case the contribution from $K = 2$ will be suppressed. Similarly, we can find that for $N_t = 5$ and for $n_0 = 1$ there are 5 steps in the I–V dependence, while for $n_0 = 2$ and 3 there are 4 and 3 steps, respectively. The position of all the steps in the I–V dependence will determine the energy structure of the trap. If we take into account the hole-phonon interaction then an additional scale in the energy spectra of the trap system and an additional structure in the I–V dependence due to the phonons should be expected.

The energy spectra of the hole-phonon quantum system, described by the Hamiltonian $\mathcal{H}_{\text{trap}}$ can be found only numerically. To find the eigenfunctions and eigenvalues of a single-hole trap system we make the system finite by introducing limitations on the total number of phonons [94] $\sum_i n_{\text{ph},i} \leq 10$, where $n_{\text{ph},i}$ is the number of phonons on site i. The energy spectra of a trap system without a hole can be easily found. In this case the Hamiltonian H_{trap} is just the Hamiltonian of free phonons at each site of the trap, so the energy of the trap system is just the sum of the energy of all phonons present in the system.

After we derive the energy spectra of the DNA Hamiltonian (5.22) without holes and with a single hole in the trap we solve the system of linear equations (5.25)–(5.26) for a given bias voltage to find the probabilities $P_{1,p}$ and $P_{0,m}$. Then we substitute this solution into (5.29) to find the stationary tunneling current under a given bias voltage. We have calculated the current (5.29) as a function of V_{sd} for different values of on-site energy, ϵ, which can be changed by the gate voltage or by doping. By varying V_{sd} we are keeping the on-site energy ϵ the same and vary the chemical potentials of the leads as $\mu_{\text{L}} = V_{\text{sd}}/2$ and $\mu_{\text{R}} = -V_{\text{sd}}/2$.

There are five dimensionless parameters which characterize the I–V dependence: the nonadiabaticity parameter [95] $\gamma = \hbar\omega/t$, with a typical value of $\sim$ 0.01–0.5 for DNA, the canonical hole-phonon coupling constant [95] $\lambda = \chi^2/(2\hbar\omega t)$ which is $\sim$ 0.2–1 for DNA, dimensionless bias voltage V_{sd}/t, on-site energy ϵ/t, and the ratio of the relaxation time and the tunneling time $\tau\Gamma_0$.

The calculations have been performed for $N_t = 2$ and $N_t = 3$, i.e., for 2 and 3 base pairs in the trap. The example of such a system could be the guanine hole traps: GG and GGG spots surrounded by adenines. In all the calculations we kept the ratio of the relaxation and the tunneling time equal to 1 ($\tau\Gamma_0 = 1$), i.e., the hole-phonon system in the trap is not in the equilibrium. Different values of $\tau\Gamma_0$, ranging from $\tau\Gamma_0 \ll 1$ (equilibrium case) to $\tau\Gamma_0 \gg 1$ (nonequilibrium case) do not modify qualitatively the behavior of the I–V curve. The phonon steps in the I–V dependence can be seen only when the temperature is less than the phonon frequency. In our calculations the temperature is equal to $0.01t$.

In Fig. 5.7, our results are shown for two base pairs (sites) in the trap. The tunneling occurs through one of the sites, $n_0 = 1$. For an uncoupled hole-phonon system the I–V dependence has two steps corresponding to two

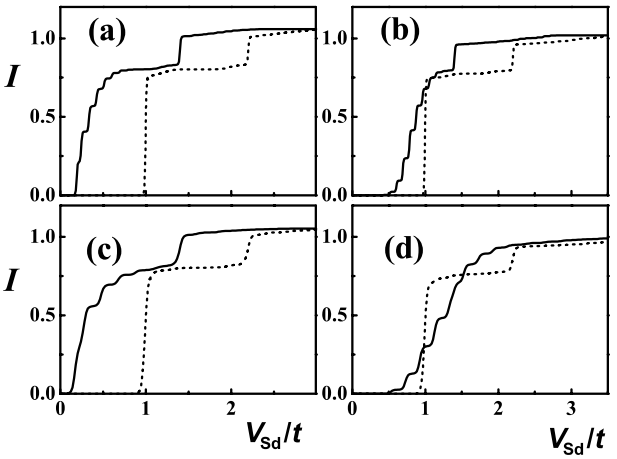

Fig. 5.7. a–d. Current vs the source-drain voltage shown for two base pairs in the trap ($N_t = 2$) and different values of phonon frequency and hole-phonon interaction strength: **a** $\gamma = 0.1$, $\lambda = 0.5$; **b** $\gamma = 0.1$, $\lambda = 1.0$; **c** $\gamma = 0.2$, $\lambda = 0.5$; **d** $\gamma = 0.2$, $\lambda = 1.0$. *Solid line* corresponds to $\epsilon = 1.3t$ while the *dashed line* is for $\epsilon = 2.7$

single-hole energy levels. The distance between the steps is $\delta V_{sd} = 2t$. For a small hole-phonon coupling constant $\lambda = 0.5$ (Fig. 5.7a,c), the additional structures of width $\delta V_{sd} \simeq \hbar\omega$ due to the phonon sidebands appear only at the first step and the second step can still be clearly distinguished. At the same time for a large gate voltage (large on-site energy ϵ), the phonon steps are suppressed and the I–V structure becomes similar to that of a zero-coupling strength, which is shown in Fig. 5.7a,c by dashed lines. For a strong hole-phonon interaction ($\lambda = 1$), the phonon steps suppress the steps due to inter-site hopping within the trap (Fig. 5.7b,d). This suppression becomes stronger for a larger non-parabolicity γ, which is illustrated in Fig. 5.7b,d by a solid line for $\gamma = 0.1$ and $\gamma = 0.2$. With increasing gate voltage the phonon steps disappear and the I–V dependence shows a clear two-step structure.

The origin of such a suppression of the phonon steps can be understood by considering the case of a very short relaxation time. If the relaxation time is much smaller than the tunneling time, then before tunneling the hole-phonon system is in equilibrium. At low temperatures this means that the system will be at the ground state, i.e., without any phonons if there are no holes in the trap and in the polaronic state when there is one hole. The tunneling current through the trap can be considered as a two-step process: the tunneling from the left contact into the trap and the tunneling from the trap into the right contact. Since we consider only the states with no more than one hole in the trap then the tunneling from the left contact will be tunneling to the state without any phonons. The final state after the tunneling will be the state of a single hole-phonon system. The condition of the tunneling is that the energy of the hole in the left contact is equal to

the energy of a single hole-phonon system, which can be either in the ground state or in the excited states. Since the tunneling rate is proportional to the overlap of the hole-phonon trap state, the state without any phonons and the hole in the n_0 site (see (5.28)), the tunneling occurs only into two states of the coupled hole-phonon system. These states are polaronic states of the hole-phonon system originated from a single hole state of the trap system without hole-phonon coupling. Therefore, the tunneling from the left contact will probe only a single-hole state, i.e. it results into a two-step structure due to hole-hopping in the I–V dependence.

Tunneling to the right contact is from the ground state of the coupled hole-phonon system. After the tunneling the trap system is just the phonon system, which can be either in the ground state or in the excited states. The energy conservation during the tunneling (see (5.27)) means that the energy of the ground state of the hole-phonon system is equal to the energy of the hole in the right contact plus the energy of the phonon state in the trap. Therefore, the tunneling from the trap into the right contact should produce the phonon steps in the I–V dependence.

Finally, tunneling from the left contact into the trap results in steps in the I–V dependence due to hole-hopping between the sites of the trap, while the tunneling from the trap into the right contact produces the steps due to the phonons. If the gate voltage or the on-site energy is increased, then when the tunneling from the left contact into the traps is allowed, the chemical potential of the right contact will be low enough. This means that after the tunneling, the trap system can be left in the state with many phonons. In terms of the phonon steps this means that the steps will be suppressed.

From Fig. 5.7, we can conclude that for typical parameters of the DNA structure the hopping integral between the sites within the DNA traps and phonon frequency which determine the energetics of the hole-phonon trap system, can be found from the dependence of the tunneling current on $V_{\rm sd}$. From a small gate voltage, the phonon frequency can be found from the I–V curve, while for a larger gate voltage, the hopping integral can be obtained.

The I–V curve should show even richer structure for a larger number of sites in the trap. In Fig. 5.8, the current as a function of the bias voltage is shown for $N_{\rm t} = 3$ sites. In this case, the tunneling is possible through the sites $n_0 = 1$ and $n_0 = 2$. For an uncoupled hole-phonon system, the I–V curve shows three steps for $n_0 = 1$ (dotted line in Fig. 5.8a), and two steps for $n_0 = 2$ (dotted line in Fig. 5.8b). This means that for $n_0 = 2$, only two states have non-zero amplitude at $n = 2$ and they contribute to the tunneling current. The finite hole-phonon coupling results in two effects: the phonon steps in the I–V dependence similar to a two-site trap (Fig. 5.7), and the polaronic effect which redistributes the hole density along the trap and increases or decreases the tunneling current.

For a small hole-phonon coupling ($\lambda = 0.5$), the phonon steps are seen only at the first hopping step (Fig. 5.8a,b (solid lines)). The separation between the steps is the phonon frequency. Similar to Fig. 5.7, an increase of the gate

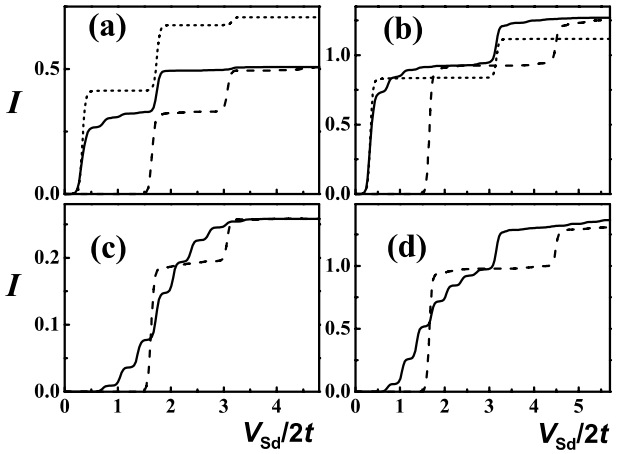

Fig. 5.8. a–d. Current vs the source-drain voltage shown for three base pairs in the trap ($N_t = 3$) and $\gamma = 0.2$, but for different tunneling points n_0 and for different values of hole-phonon interaction strength: **a** $n_0 = 1$: $\lambda = 0.5$ and $\epsilon = 1.7t$ (*solid line*), $\lambda = 0.5$ and $\epsilon = 3.0t$ (*dashed line*), $\lambda = 0$ and $\epsilon = 1.7t$ (*dotted line*); **b** $i_0 = 2$: $\lambda = 0.5$ and $\epsilon = 1.7t$ (*solid line*), $\lambda = 0.5$ and $\epsilon = 3.0t$ (*dashed line*), and $\lambda = 0$, $\epsilon = 1.7t$ (*dotted line*); **c** $i_0 = 1$: $\lambda = 1$ and $\epsilon = 1.7t$ (*solid line*), $\epsilon = 3.0t$ (*dashed line*), **d** $i_0 = 2$: $\lambda = 1$ and $\epsilon = 1.7t$ (*solid line*), $\epsilon = 3.0t$ (*dashed line*)

voltage (the on-site energy) suppresses the phonon steps and the I–V curve becomes similar in structure to the uncoupled case (Fig. 5.8a,b, dashed lines). The main difference between the coupled and the uncoupled systems is the different amplitude of the steps. This difference is due to the redistribution of the hole within the trap due to the interaction with the phonons. This results in a suppression of the tunneling current when the tunneling occurs through the site $n_0 = 1$ and enhancement of the tunneling current for $n_0 = 2$ (Fig. 5.8a,b). Therefore, the interaction with the phonons or the polaronic effect increases the probability for the hole to occupy the site $n = 2$.

For a larger hole-phonon coupling ($\lambda = 1$), the steps due to the hole-hopping almost completely disappear for $n_0 = 1$ (Fig. 5.8c, solid line), but some structure is still visible for $n_0 = 2$ (Fig. 5.8d, solid line). As we mentioned above, with increasing gate voltage the phonon steps should be suppressed and the I–V structure should clearly show the steps due to the hole hopping between the sites of the trap. This behavior is illustrated in Fig. 5.8c,d by dashed lines.

To illustrate the polaronic effects due to the hole-phonon coupling which is clearly seen in Fig. 5.8, we have calculated the density of holes and the average number of phonons within the traps for different strengths of the hole-phonon interaction. The results are shown in Fig. 5.9. With increasing hole-phonon interaction, the hole states become more localized at the center of the trap (see Fig. 5.9), i.e. we observe the polaronic effect in the trap system.

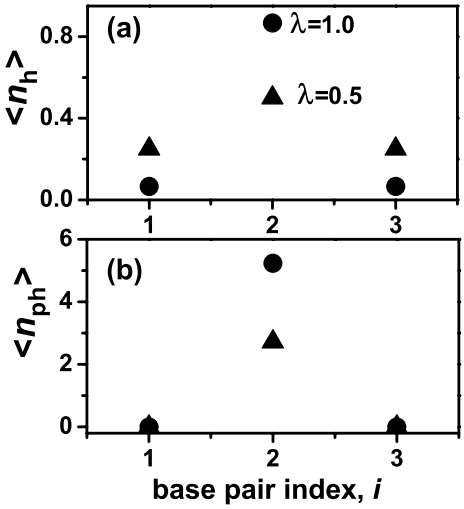

Fig. 5.9. a,b. The average number of holes (**a**) and the average number of phonons (**b**) for a single-hole system in a GGG trap, shown as a function of the base index. *Dots* and *triangles* corresponds to the hole-phonon interaction strength $\lambda = 1.0$ and 0.5, respectively

Localization of the hole at the center of the trap results in an increase of the tunneling current for tunneling through the central site of the trap $n_0 = 2$ (see Fig. 5.8b,d), and a decrease of the tunneling current through $n_0 = 1$ (see Fig. 5.8a,c). In addition to the changes to the tunneling current, the polaronic effect also modifies the structure of the I–V curve. This can be seen in Fig. 5.8a, where increasing the hole-phonon interaction, the third step due to the hole hopping disappears. Therefore, in the hole-phonon coupled system with $N_t = 3$, only two steps due to the hole hopping can be clearly seen in the I–V dependence at a large gate voltage.

5.7.3 Bipolaron Formation in a DNA Molecule

In the previous subsections, we disregarded the Coulomb blockade, the effects related to the hole-hole interactions. Therefore, we assumed the trap system can be occupied only by a single hole. This assumption is valid as long as the repulsion between the holes is quite strong. The specific feature of the hole-phonon system is that the repulsion between the holes can be strongly suppressed in such systems and might even result in an effective attraction between the holes. If there is an attraction between the holes then the trap with the two holes should have a lower energy than the trap with a single hole. Such energetics should modify the I–V dependence of the transverse tunneling current. To study this problem, we first analyze the condition of the trapping of two holes by the trapping spots, such as a GG, GGG, or

GGGG. The formation of the bound state of two holes trapped by the G-sites is analogous to bipolaron formation in the homogeneous one-dimensional system [96].

To write the Hamiltonian of a many-hole system within a trap, we need to add to the single-particle Hamiltonian (5.22) the term which describes the Coulomb interaction between the holes. Therefore, now the Hamiltonian of the hole system within a trap consists of three parts: (i) the tight-binding Hamiltonian which includes the hole-hopping between the nearest base pairs and the on-site energies of a hole, (ii) the hole-hole interaction Hamiltonian, and (iii) the Holstein's phonon Hamiltonian with the diagonal hole-phonon interaction [78]

$$\mathcal{H}_{\rm trap} = \mathcal{H}_{\rm t} + \mathcal{H}_{\rm i} + \mathcal{H}_{\rm ph} \ , \tag{5.32}$$

with

$$\mathcal{H}_{\rm t} = \sum_{i,\sigma} \epsilon_i c^{\dagger}_{i,\sigma} c_{i,\sigma} - t \sum_{i,\sigma} \left[c^{\dagger}_{i,\sigma} c_{i+1,\sigma} + h.c. \right] \ , \tag{5.33}$$

$$\mathcal{H}_{\rm i} = \sum_{i,j,\sigma} V_{i,j} n_{i,\sigma} n_{j,-\sigma} + \sum_{i,j\neq i,\sigma} V_{i,j} n_{i,\sigma} n_{j,\sigma} \ , \tag{5.34}$$

$$\mathcal{H}_{\rm ph} = \hbar\omega \sum_{i} b^{\dagger}_i b_i + \chi \sum_{i,\sigma} c^{\dagger}_{i,\sigma} c_{i,\sigma} \left(b^{\dagger}_i + b_i \right) \ , \tag{5.35}$$

where $c_{i,\sigma}$ is the annihilation operator of a hole with spin σ on site i, and $n_{i,\sigma} = c^{\dagger}_{i,\sigma} c_{i,\sigma}$. The Hamiltonian (5.21) without the phonon part $\mathcal{H}_{\rm ph}$ was studied for a homogeneous system in [34].

In the tight-binding Hamiltonian (5.33), we assume that the site i can be either an adenine or a guanine. We then take the on-site energy of the hole at adenine (A) site as the zero energy, i.e. $\epsilon_{\rm A} = 0$, and the on-site energy of the hole at the guanine (G) site to be negative, $\epsilon_{\rm G} = -\Delta_{\rm GA} < 0$. In the interaction Hamiltonian $\mathcal{H}_{\rm i}$, we take into account only the Hartree interaction between the holes. The first term in (5.34) describes the repulsion between the two holes with different spin. The holes can then occupy the same site. The second term in (5.34) corresponds to the repulsion between the two holes with the same spin. To get the basic idea about the typical range of the interaction parameters resulting in the formation of a bound state of two holes within the region of the G-trap, we introduce a single-parameter interaction potential of the form

$$V_{i,j} = V_0 \left[(i-j)^2 + 1 \right]^{\frac{1}{2}} \ , \tag{5.36}$$

where V_0 is the on-site repulsion between the two holes. The form of the interaction potential, $V_{i,j}$, (5.36) takes into account the finite spreading of the hole on-site wave function. This spreading is about the distance between the nearest base pairs. Although the actual dependence of the interaction potential on the separation between the holes is more complicated [97] than (5.36), this difference is not important for our analysis since only the on-site

interaction plays the main role in the formation of the bound state of two holes [98].

Similar to the analysis in the previous subsection, we include in the hole-phonon Hamiltonian only the optical phonons with diagonal hole-phonon interaction, and do not take into account the acoustic phonons which results in non-diagonal hole-phonon interaction [99, 100], i.e. modify the tunneling integral. In (5.33)–(5.35), we also assumed that the hopping integral t, the phonon frequency ω, and the hole-phonon coupling constant χ, do not depend on the specific type of the base pairs (A or G).

The form of the total Hamiltonian, (5.32)–(5.35), leads to four dimensionless parameters which characterize the system: the nonadiabaticity parameter [95] $\gamma = \hbar\omega/t$, the canonical hole-phonon coupling constant [95] $\lambda = \chi^2/(2\hbar\omega t)$, dimensionless hole-hole interaction strength V_0/t, and the dimensionless difference between on-site energies of G and A, $\delta_{\rm GA} = \Delta_{\rm GA}/t$.

We determine the eigenfunctions and eigenvectors of the hole-phonon system numerically by exactly diagonalizing the Hamiltonian (5.32)–(5.35) for a finite size system consisting of six base pairs (sites). We also introduce limitations on the total number of phonons [94], $\sum_i n_{{\rm ph},i} \leq N_{\rm max}$. To compare the energy spectrum of the systems with different number of holes, we keep the maximum number of phonons *per hole* the same for all the systems. Therefore, for the two-hole system the maximum number of phonons is $N_{\rm max} = 16$ and for the one-hole system $N_{\rm max} = 8$.

Our finite size system contains six sites which are originally adenines. We then introduce the G-traps with a different number $N_{\rm G}$ of guanines, G, GG, GGG, and GGGG, in the middle of the system. For example the system with two guanines is AAGGAA. For different traps we calculate the energy of the ground state of the systems with one and two holes. There are different ways to define the bound state of two holes within the trap. The first one is based on the analysis of the hole density distribution within the trap. When the two holes occupy the same site then we can tell that this is the bound state of the two-hole system. The second one is based on energetics of the two-hole system. Denoting the corresponding energies of the hole system as $E_{1,N_{\rm G}}$ (for the one-hole system with $N_{\rm G}$ guanines) and $E_{2,N_{\rm G}}$ (for the two-hole system with $N_{\rm G}$ guanines), we can write the energetic condition that the trap with $N_{\rm G}$ guanines will accommodate two holes as

$$E_{2,N_{\rm G}} < E_{1,N_{\rm G}} + E_{1,1} \tag{5.37}$$

or

$$E_{2,N_{\rm G}} < E_{1,N_{\rm G}} + E_{1,N_{\rm G}} \ . \tag{5.38}$$

The meaning of the first condition (5.37) is as follows [101]: If the two holes are injected initially into the single guanine traps ($N_{\rm G} = 1$) of the DNA and then one of the holes is trapped by the $N_{\rm G}$ trap, then the condition (5.37) means that the second hole will also be trapped by the same $N_{\rm G}$ trap. This

condition corresponds to the experimental realization of the injection of the holes into the DNA molecule.

The second condition (5.38) is relevant to the transverse tunneling experiments. This condition actually means that if the first hole tunnels into the trap system then the second hole can also tunnel into the same trap system, i.e. the energy of a two-hole system is less than twice the energy of a single-hole system.

Since we are interested in the transverse tunneling current, we concentrate below on the condition (5.38) for the bound state of two holes. The condition (5.38) will determine the critical value of the hole-hole interaction strength, $V_0^{\rm cr}$. That means for $V_0 < V_0^{\rm cr}$ two holes will be trapped by the same trap with $N_{\rm G}$ guanines. For $V_0 > V_0^{\rm cr}$ such a trapping is energetically unfavorable.

For our investigation of the system (5.21)–(5.24), we consider the following typical DNA parameters: $0.1\,{\rm eV} < t < 0.3\,{\rm eV}$, $0.1\,{\rm eV} < \Delta_{\rm GA} < 0.5$ [102, 103], $0.05\,{\rm eV} < \hbar\omega < 0.1\,{\rm eV}$. For the dimensionless canonical hole-phonon coupling constant we have taken the value $\lambda = 1$. For this coupling constant, the size of the polaron is about 2–3 base pairs. Our calculations show that the critical value $V_0^{\rm cr}$ is very small ($V_0^{\rm cr} \approx 0.1\,{\rm eV}$) when two holes have the same spin and they can not occupy the same site. This small value of $V_0^{\rm cr}$ also illustrates the fact that the phonon mediated attraction between the holes is largest when the holes occupy the same site. Therefore, in what follows we shall consider only the case of two holes with opposite spin.

In Fig. 5.10, the ground state energy of a single hole is plotted as a function of the hole-phonon coupling constant, λ, for different types of traps. For $\lambda \approx 1$, the difference between the bound state of a hole in G and GG traps is about 0.03 eV, which is smaller than the value (0.05 eV) obtained in [104]. The size of the polaron in our calculations is 2–3 base pairs depending on the values of t and ω.

Following the condition (5.38), we need to compare the energy of a single-hole system with the energy of a two-hole system. In Fig. 5.11, the ground state energy $E_{2,N_{\rm G}}$ of two holes bound in a single trap is plotted for $N_{\rm G} = 3$

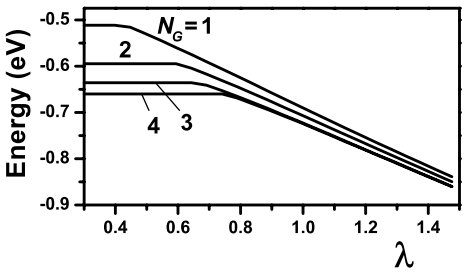

Fig. 5.10. The ground state energy of a single hole in a trap containing $N_{\rm G}$ guanines is shown as a function of the hole-phonon coupling constant, λ at $t = 0.2\,{\rm eV}$ and $\Delta_{\rm GA} = 0.3\,{\rm eV}$. The numbers next to the lines are the number of guanines in the trap

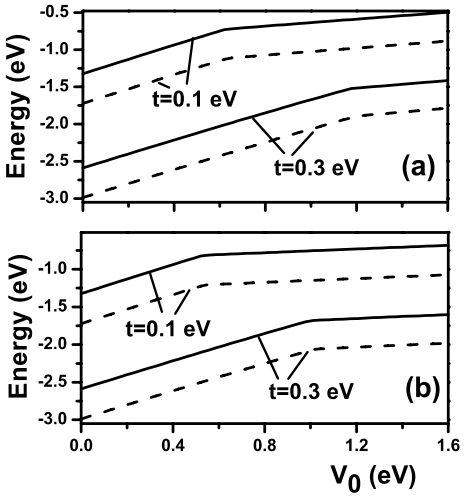

Fig. 5.11. a,b. Ground state energy of two holes in the trap containing $N_{\rm G} = 3$ guanines (**a**) and $N_{\rm G} = 4$ guanines (**b**) as a function of the inter-hole interaction strength, V_0, for $\Delta_{\rm GA} = 0.3\,{\rm eV}$ (*solid line*) and $\Delta_{\rm GA} = 0.5\,{\rm eV}$ (*dashed line*)

(Fig. 5.11a) and for $N_{\rm G} = 4$ (Fig. 5.11b) as a function of the hole-hole interaction strength for different values of $\Delta_{\rm GA}$ and t. Here we notice that at some critical value $V_0^{\rm b}$ of the hole-hole interaction strength, there is a change of slope in the $E_{2,N_{\rm G}}(V_0)$ dependence. This critical value corresponds to the condition that the two holes are bound in the G-traps, forming a bipolaron. The bound state in this case means that the holes are at the same site of the trap. The illustration of this fact is given in Fig. 5.12. In Fig. 5.12a the average number of holes, $\langle n_{\rm h}\rangle = \langle n_{i,\sigma}\rangle + \langle n_{i,-\sigma}\rangle$, is shown as a function of the base pair index for a GGGG trap and two different values of the hole-hole interaction strength, V_0. It is clearly seen that for $V_0 = 0.8\,{\rm eV} < V_0^{\rm b}$, the two holes are almost at the same G sites, while at $V_0 = 1.2\,{\rm eV} > V_0^{\rm b}$ the holes are away from each other. The corresponding distribution of the average number of phonons $\langle n_{\rm ph}\rangle$, is shown in Fig. 5.12b.

Another critical value of V_0 is introduced by the equation (5.38). The competition between $2E_{1,N_{\rm G}}$ and $E_{2,N_{\rm G}}$ is illustrated in Fig. 5.13. Comparing the energies $2E_{1,N_{\rm G}}$ and $E_{2,N_{\rm G}}$ for $\lambda = 1$ and different values of t, $\Delta_{\rm GA}$, and ω, one can determine $V_0^{\rm cr}$. The result is summarized in Table 5.1 for the GGGG trap. The corresponding results for the GGG trap gives about 0.1 eV smaller values for $V_0^{\rm cr}$. The dimensionless parameters, γ, $\delta_{\rm GA}$, and $V_0^{\rm cr}/t$, are also given in Table 5.1. From these data we can conclude that within the present range of parameters the dependence of $V_0^{\rm cr}$ on $\Delta_{\rm GA}$ is weak, and $V_0^{\rm cr}/t$ depends mainly on γ. This dependence can be approximated by a linear function as

$$V_0^{\rm cr} \approx 2.3\gamma t + 1.6t \approx 2.33\hbar\omega + 1.6t\,. \tag{5.39}$$

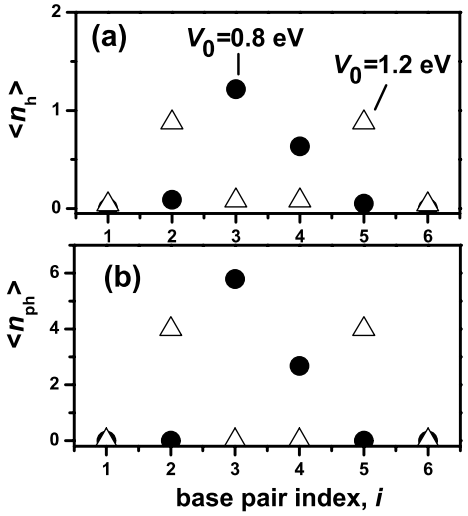

Fig. 5.12. a,b. The average number of holes (**a**) and the average number of phonons (**b**) for a two hole system in a GGGG trap are shown as a function of the base index. The tunneling integral is $t = 0.3\,\text{eV}$ and the hole-phonon coupling is $\lambda = 1$. *Dots* and *triangles* corresponds to inter-hole interaction strength $V_0 = 0.8\,\text{eV}$ and $1.2\,\text{eV}$ respectively

Table 5.1. Calculated values of V_0^{cr} for various values of the dimensionless DNA parameters

t (eV)	$\hbar\omega$ (eV)	Δ_{GA} (eV)	V_0^{cr} (eV)	γ	δ_{GA}	V_0^{cr}/t
0.1	0.1	0.1	0.38	1.00	1.00	3.8
0.1	0.1	0.3	0.41	1.00	3.00	4.1
0.1	0.1	0.5	0.43	1.00	5.00	4.3
0.1	0.05	0.1	0.32	0.50	1.00	3.2
0.2	0.1	0.1	0.48	0.50	0.50	2.4
0.2	0.1	0.3	0.56	0.50	1.50	2.8
0.2	0.1	0.5	0.58	0.50	2.50	2.9
0.3	0.1	0.1	0.78	0.33	0.33	2.6
0.3	0.1	0.3	0.75	0.33	1.00	2.5
0.3	0.1	0.5	0.80	0.33	1.67	2.7
0.3	0.05	0.3	0.54	0.17	1.00	1.8
0.3	0.05	0.5	0.58	0.17	1.67	1.9

The condition (5.37) of formation of the bound state of two holes within the guanine traps gives the higher [101] critical values of the on-site hole-hole repulsion potential, V_0^{cr}, by approximately $0.3\,\text{eV}$.

We see from these data that depending on the parameters of DNA, the critical hole-hole interaction strength V_0^{cr} can range from $0.3\,\text{eV}$ to $0.8\,\text{eV}$.

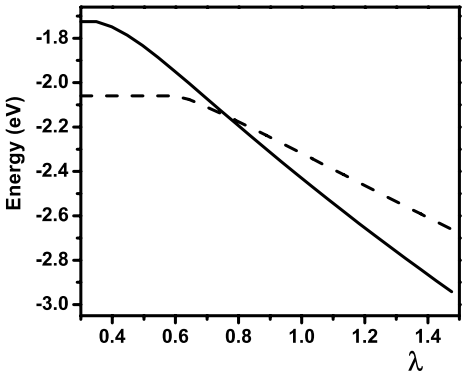

Fig. 5.13. Energies $2E_{1,4}$ and $E_{2,4}$ of a two-hole system are shown as a function of hole-phonon coupling, λ, by *dashed* and *solid lines*, respectively. Tunneling integral is $t = 0.3\,\text{eV}$ and $\Delta_{\text{GA}} = 0.3\,\text{eV}$

Numerical analysis of the electron correlations in different types of DNA [97] shows that the hole-hole interaction strength is around 0.9 eV for A-DNA and 1.5 eV for B-DNA. Additional suppression of the inter-hole interaction by a factor of ≈ 0.7 [77] can occur for DNA in solution, when hole-hole interaction is screened by polar solvent molecules and mobile counterions. Under this condition trapping of two holes by GGG and GGGG traps would be possible. Formation of the bound state of two holes at the G-traps requires also a strong hole-phonon interaction, which should overcome the hole-hole Coulomb repulsion. In our calculations, the hole-phonon coupling constant was $\lambda = 1$ which is larger than the experimentally reported $\lambda \approx 0.2$ in Ref. [105]. Hence, experimental observation of the two-hole bound state should give an additional estimate for the strength of hole-phonon interaction.

5.7.4 Pair Tunneling

Experimental observation of the bipolaron formation within the DNA traps should provide additional information about the internal parameters of the DNA molecule, such as the hole-hole repulsion strength, the hole-phonon coupling constant and others. In this section, we discuss the possible manifestation of the bipolaron in the transverse tunneling experiments. We show below that the presence of a bound state of two holes results in the specific I–V dependence of the tunneling current.

Formation of the bound state of two holes within the guanine trap means that the energy of the two holes in the trap is less than the energy of a single hole. This fact results in a modification of the I–V dependence of the tunneling current. Indeed, since there is energy conservation during the tunneling the energy of the hole in the contact should be equal to the energy of the hole in

the trap. This means that if the bipolaron has a lower energy than a single hole, then the tunneling of two holes [106] simultaneously becomes more energetically favorable than the tunneling of a single hole.

To illustrate the manifestation of pair tunneling in the transverse tunneling experiments, we consider below a simple model. In this model, we assume that there is no phonon in the system, but there is an effective attraction between the holes, i.e. the energy of two holes is less then the energy of a single hole in the trap. We will also concentrate only on the competition between the contributions of the two-hole states and a single-hole state into the tunneling current and assume that the trap system has a single two-hole level and a single one-hole level. In this case the corresponding rate equations take the form

$$\begin{aligned}
\frac{dP_0}{dt} &= -\left(W_{0\to1} + W_{0\to2}\right) P_0 + W_{1\to0} P_1 + W_{2\to0} P_2 \\
\frac{dP_1}{dt} &= W_{0\to1} P_0 - \left(W_{1\to0} + W_{1\to2}\right) P_1 + W_{2\to1} P_2 \\
\frac{dP_2}{dt} &= W_{0\to2} P_0 + W_{1\to2} P_1 - \left(W_{2\to1} + W_{2\to0}\right) P_2 \ ,
\end{aligned} \tag{5.40}$$

where P_0, P_1, and P_2 are the probability that there are no holes, one hole, and two holes in the trap, respectively. These probabilities should also satisfy the normalization condition $P_0 + P_1 + P_2 = 1$. The transition rates in the system of linear equations (5.40) can be written as

$$\begin{aligned}
W_{1\to0} &= \Gamma_1 \left[1 - f_{\mathrm{L}}(E_1) + 1 - f_{\mathrm{R}}(E_1)\right] \\
W_{0\to1} &= \Gamma_1 \left[f_{\mathrm{L}}(E_1) + f_{\mathrm{R}}(E_1)\right] \\
W_{1\to2} &= \Gamma_1 \left[f_{\mathrm{L}}(E_2 - E_1) + f_{\mathrm{R}}(E_2 - E1)\right] \\
W_{2\to1} &= \Gamma_1 \left[1 - f_{\mathrm{L}}(E_2 - E_1) + 1 - f_{\mathrm{R}}(E_2 - E1)\right] \\
W_{2\to0} &= \Gamma_2 \sum_{i,j} \{\left[1 - f_{\mathrm{L}}(\epsilon_i)\right] \left[1 - f_{\mathrm{L}}(\epsilon_j)\right] \\
&\quad + \left[1 - f_{\mathrm{R}}(\epsilon_i)\right] \left[1 - f_{\mathrm{R}}(\epsilon_j)\right] \\
&\quad + \left[1 - f_{\mathrm{L}}(\epsilon_i)\right] \left[1 - f_{\mathrm{R}}(\epsilon_j)\right]\} \, \delta\left(\epsilon_i + \epsilon_j - E_2\right) \\
W_{0\to2} &= \Gamma_2 \sum_{i,j} \Big\{ f_{\mathrm{L}}(\epsilon_i) f_{\mathrm{L}}(\epsilon_j) + \\
&\quad f_{\mathrm{R}}(\epsilon_i) f_{\mathrm{R}}(\epsilon_j) f_{\mathrm{L}}(\epsilon_i) f_{\mathrm{R}}(\epsilon_j) \Big\} \, \delta\left(\epsilon_i + \epsilon_j - E_2\right) \ ,
\end{aligned}$$

where Γ_1 and Γ_2 are the tunneling rates for one- and two-hole tunneling, and E_1 and E_2 are the energies of one hole and two hole systems, respectively. Here the energy E_2 takes into account the interaction between the holes and can be expressed in terms of the bound energy, Δ_{B}, of two holes as $E_2 = 2E_1 - \Delta_{\mathrm{B}}$. When the ground state of the two hole system is a bipolaron then $\Delta_{\mathrm{B}} > 0$, otherwise $\Delta_{\mathrm{B}} < 0$.

We can see from the expression for the transition rates that the specific feature of the pair tunneling is the presence of the sum over the hole states in the contacts. This sum should modify the dependence of the transition rates on the chemical potentials of the contacts and, correspondingly, on the bias voltage. If we assume that the density of states of the hole in the contacts is constant, then the transition rate corresponding to the tunneling of a single hole from the contact into the trap will not depend on the chemical potential. The transition rate corresponding to the tunneling of two holes from the same contact into the trap will be proportional to the chemical potential, i.e., $\propto (2\mu_{\rm s} - E_2)$, while the transition rate of the two hole tunneling from different contacts will not depend on the chemical potential of the contacts. The dependence of the transition rates on the chemical potential and the bias voltage results in the special structure of I–V characteristics for the systems with pair tunneling.

Under the given bias and gate voltages, the stationary solution of the linear system of equations (5.40) can be found and the corresponding tunneling current can be calculated from the following expression

$$I = [W_{\mathrm{R},1\to 0} - W_{\mathrm{R},1\to 2}]\, P_1 + 2W_{\mathrm{R},2\to 0} P_2 - [W_{\mathrm{R},0\to 1} + W_{\mathrm{R},0\to 2}]\, P_0 \ . \quad (5.41)$$

The I–V characteristics has been found for different gate voltages and different ratios Γ_2/Γ_1. Since the tunneling rate Γ_2 corresponds to the pair tunneling it is smaller than Γ_1. Below we assume that at zero bias and zero gate voltage, the chemical potentials of the contacts coincide with the energy level of a single hole in the trap, i.e. E_1. In this case it is convenient to measure the bias voltage and the gate voltage in the units of $\Delta_{\rm B} = 2E_1 - E_2$. The results of the calculations are shown in Figs. 5.14 and 5.15 for $\Delta_{\rm B} > 0$ and $\Delta_{\rm B} < 0$, respectively. For a positive $\Delta_{\rm B}$, i.e. when the bound state of

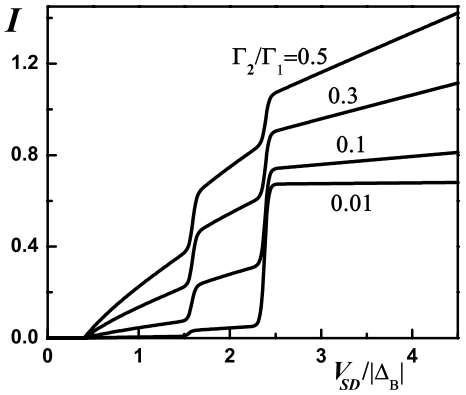

Fig. 5.14. Current vs bias voltage is shown for $\Delta_{\rm B} > 0$ and for different values of ratio Γ_2/Γ_1. The gate voltage is $0.2\Delta_{\rm B}$ and the temperature is $0.01\Delta_{\rm B}$. The ground state of the trap is the bound state of two holes

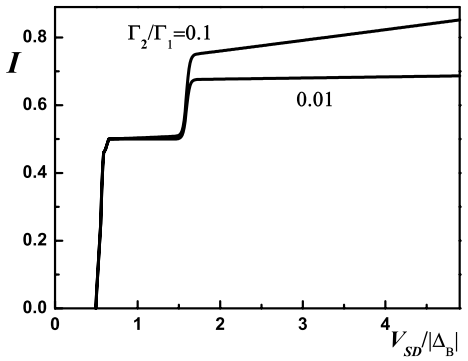

Fig. 5.15. Current vs bias voltage is shown for $\Delta_B < 0$ and for different values of ratio Γ_2/Γ_1. The gate voltage is $0.2\Delta_B$ and the temperature is $0.01\Delta_B$. The ground state of the trap is a single-hole state

two holes has the lower energy than a single-hole state, the I–V structure has a clear linear dependence on the bias voltage within the whole region of the parameters (Fig. 5.14). There are two steps in the I–V dependence, where each step corresponds to the opening of an additional channel for tunneling. In what follows, we analyze these channels in more detail. The variation of Γ_2/Γ_1 has a strong effect on the I–V curve. With decreasing Γ_2/Γ_1, the contribution of the pair tunneling becomes suppressed and at a very small Γ_2/Γ_1 only a single step due to a single-hole tunneling can be seen in the I–V dependence.

The behavior of the I–V dependence becomes very different at $\Delta_B < 0$ (Fig. 5.15). In this case we also have two steps. Now the first step is due to a single-hole tunneling, while the second step is due to a combination of pair tunneling and a single-hole tunneling. At a high bias voltage, i.e. within a second step, we can see the linear dependence in the I–V characteristics, which is a specific feature of the pair tunneling of the holes. With a decrease of the ratio Γ_2/Γ_1, the pair tunneling and correspondingly, the linear dependence becomes suppressed, but still the structure has the two steps. Now the second step is entirely due to a single-hole tunneling and is a manifestation of the Coulomb blockade.

The origin of the different steps at $\Delta_B > 0$ is analyzed in Fig. 5.16, where the occupations of the levels of the traps are shown as a function of bias voltage. The gate voltage is $V_g = 0.2\Delta_B$ and at the zero bias voltage, the trap is occupied by two holes. With an increase of the bias voltage, tunneling to the left contact becomes allowed and we can see the linear dependence of the tunneling current on the bias voltage. The trap is partially occupied by two holes, and only the pair-tunneling contributes to the tunneling current. With an additional increase of the bias voltage, the Fermi level of the right contact becomes equal to the energy of a single-hole state in the trap and the tunneling of a single hole becomes energetically allowed. These results in

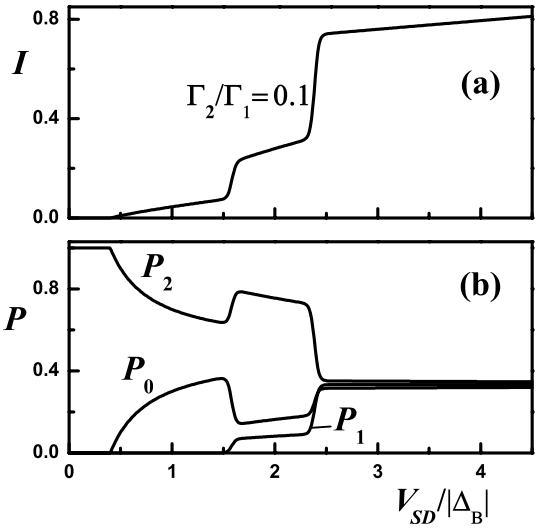

Fig. 5.16. a Current vs the bias voltage, shown for $\Delta_B > 0$, $\Gamma_2/\Gamma_1 = 0.1$, and gate voltage $V_g = 0.2\Delta_B$. **b** The corresponding probabilities, P_0, P_1, and P_2, are shown as a function of the bias voltage. The ground state of an isolated trap is the bound state of two holes

the first step of the I–V curve. Within this region we have the pair-tunneling and a single-hole tunneling to the empty trap or from the trap occupied by a single hole. The origin of the second step at a higher bias voltage is the opening of an additional channel for tunneling: the single-hole tunneling

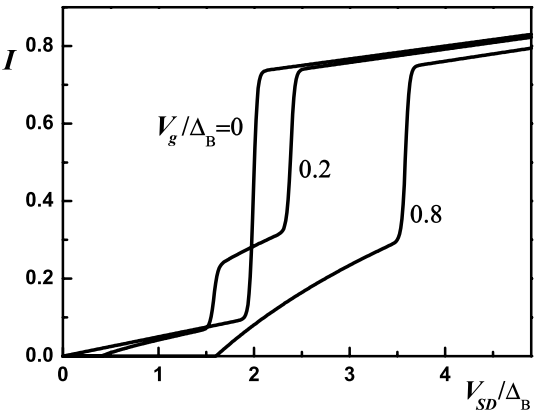

Fig. 5.17. Current vs bias voltage is shown for $\Delta_B > 0$ and for different values of gate voltage V_g. The ratio of the pair tunneling rate and a single-hole tunneling rate is $\Gamma_2/\Gamma_1 = 0.1$. The temperature is $0.01\Delta_B$. The ground state of the trap is the bound state of two holes

from the two-hole state in the trap. Finally, the shape of the I–V curve is determined by the following three channels of tunneling: pair tunneling, a single-hole tunneling to the empty trap or from a single-hole state of the trap, and a single-hole tunneling from the two-hole state of the trap or to a single-hole state of the trap. The opening of different channels depends on the gate voltage. Therefore, by variation of the gate voltage we can modify the I–V structure of the tunneling current through the DNA trap. In Fig. 5.17, different possible I–V dependencies are shown at different gate voltages. At small and high gate voltages there is only a single step in the I–V curve, while at an intermediate gate voltage there are two steps.

5.8 Summary

Many experimental measurements of charge migration along DNA have been carried out in the last decade, especially after the direct measurement of DNA conductance became available. The apparently diverse conclusions extracted from different experiments have made it imperative to initiate systematical and comprehensive theoretical efforts for fundamental understanding of the underlying mechanisms for the charge transfer in DNA. One focus of these efforts is the mechanistic understanding of the observed weak distance dependence of charge transfer along a DNA with the specific sequence: $(\mathrm{G{:}C})(\mathrm{T{:}A})_{\mathcal{M}}(\mathrm{G{:}C})_3$. Previously, thermally-induced hopping mechanism was invoked to explain it by many authors. In this mechanism, strong dephasing effects is assumed to introduce phase incoherence in the spatial scale of a nanometer. We have proposed that the phase coherence is maintained in the nano-scale of distance in DNA but the two-stranded geometry plays an important role in the weak distance dependence. In other words, the distance dependence is a geometrical characteristic of the quantum transport rather than a trivial property of the classical transport. Within this framework, a quantitative analysis based on the multichannel superexchange mechanism successfully explains the main feature of the experimental result and makes some predictions for future experiments. In the existing experiment, a critical number $\mathcal{M}_{\mathrm{c}} = 3$ is observed when the crossover from strong to weak distance dependence occurs. For the multichannel superexchange mechanism, this crossover number depends on the ratio of the intra- to interstrand coupling parameter in DNA. A crossover number different from three may be observed in other experiments.

The experimental analysis of the transverse transport through a DNA trap can provide additional information about the parameters of the DNA molecule. The dependence of the tunneling current on the applied bias voltage has a staircase structure. The shape of the structure can be changed by applying the gate voltage to the trap. If the repulsion between the holes within the trap is strong then the main mechanism of tunneling is a single-hole tunneling. In this case, the staircase structure of the I–V dependence has

two types of steps: the first one is due to the hole hopping between the sites of the trap, while the second one is due to hole-optical phonon interactions, i.e. the phonon sidebands. At a small gate voltage, both types of steps are present in the I–V dependence and the phonon frequency can be extracted from the I–V curve. At a large gate voltage, the phonon steps become strongly suppressed and the steps due to hole hopping can be clearly seen in the I–V dependence. In this case the width of the steps gives the value of the hopping integral between the sites of the trap.

The transverse tunneling measurements can also be used to analyze the possibility for formation of the bipolaron, i.e. the bound state of the two holes (polarons), within the DNA trap. If the bound state of two holes has a lower energy than a single-hole state then the main contribution to the tunneling current at a low bias voltage comes from the pair tunneling of two holes. This tunneling process results in a specific dependence of the tunneling rate on the bias voltage. As a result of this dependence the I–V curve in the case of a bipolaron formation can be distinguished from the I–V curve corresponding to a single-hole tunneling.

Acknowledgement. This work has been supported by the Canada Research Chair Program and a Canadian Foundation for Innovation (CFI) Grant.

References

1. K.B. Beckman and B.N. Ames, J. Biol. Chem. **272**, 19633 (1997); S. Loft and H.E. Poulsen, J. Mol. Med. **74**, 297 (1996); A.P. Grollman and M. Moriya, Trends in Genetics **9**, 246 (1993); C.J. Burrows and J.G. Muller, Chem. Rev. **98**, 1109 (1998).
2. E. Braun and K. Keren, Adv. Phys. **53**, 441 (2004).
3. C. Dekker and M.A. Ratner, Phys. World **14**, (8), 29 (2001).
4. J. Lagerqvist, M. Zwolak and M. Di Ventra, Nano Letters **6**, 779 (2006).
5. M. Xu, R.G. Endres and Y. Arakawa, Chapter 9, this volume.
6. M. Zwolak and M. Di Ventra, Nano Letters **5**, 421 (2005).
7. K.F. Herzfeld, J. Chem. Phys. **10**, 508 (1942).
8. J. Ladik, Acta Phys. Acad. Sci. Hung. **11**, 239 (1960).
9. D.D. Eley and D.I. Spivey, Trans. Faraday Soc. **58**, 411 (1962).
10. K.V. Mikkelsen and M. A. Ratner, Chem. Rev. **87**, 113 (1987); M.D. Newton, Chem. Rev. **91**, 767 (1991).
11. R.A. Marcus, Rev. Mod. Phys. **65**, 599 (1993).
12. D.N. Beratan, J. Betts and J.N. Onuchic, Science **252**, 1285 (1991); J. Evenson, M. Karplus, Science **262**, 1247 (1993); S. Steenken, S.V. Jovanovic, J. Am. Chem. Soc. **119**, 617 (1997); S.O. Kelley and J.K. Barton, Chem. Biol. **5**, 413 (1998); M. Ratner, Nature **397**, 480 (1999); E. Boone and G.B. Schuster, Nucleic Acids Res. **30**, 830 (2002); D.M. Adams, et al., J. Phys. Chem. B **107**, 6668 (2003).

13. R.G. Endres, D.L. Cox and R.R.P. Singh, Rev. Mod. Phys. **76**, 195 (2004).
14. G.B. Schuster (Ed.), Long-range charge transfer in DNA, Springer-Verlag, Berlin Heidlberg, (2004).
15. J. Jortner and M. Bixon, (Eds.), Electron transfer: from isolated molecules to biomolecules, Part Two, John Wiley & Sons, Inc., (1999).
16. D. DeVault, Quantum-mechanical tunnelling in biological systems, 2nd ed., Cambridge University Press, (1984).
17. G. Fischer, Vibronic Coupling, Academic Press, (1984).
18. C.R. Calladine, H.R. Drew, B.F. Luisi and A.A. Travers, Understanding DNA (Elsevier, London, 2004); J.D. Watson, et al., Molecular Biology of the Gene, (Benjamin Cummings, San Francisco, 2004), 5th edition; B. Alberts, et al., Molecular Biology of the Cell, (Garland Science, New York, 2002), 4th edition.
19. H. Sugiyama and I. Saito, J. Am. Chem. Soc. **118**, 7063 (1996).
20. H.Y. Zhang, X.Q. Li, P. Han, X.Y. Yu and Y.J. Yan, J. Chem. Phys. **117**, 4578 (2002).
21. E. Artacho, M. Machado, D. Sanchez-Portal, P. Ordejon, and J. M. Soler, Mole. Phys. **101**, 1587 (2003).
22. E. Maciá, F. Triozon and S. Roche, Phys. Rev. B **71**, 113106 (2005).
23. W. Ren, J. Wang, Z.S. Ma and H. Guo, Phys. Rev. B **72**, 035456 (2005).
24. S.D. Wetmore, R.J. Boyd and L.A. Eriksson, Chem. Phys. Lett. **322**, 129 (2000).
25. A.A. Voityuk, J. Jortner, M. Bixon and N. Rösch, J. Chem. Phys. **104**, 9740 (2000); ibid. **114**, 5614 (2001).
26. A. Troisi and G. Orlandi, Chem. Phys. Lett. **344**, 509 (2001).
27. R. Di Felice, A. Calzolari, E. Molinari and A. Garbesi, Phys. Rev. B **65**, 045104 (2002).
28. J. Rak, A.A. Voityuk, A. Marquez and N. Rösch, J. Phys. Chem. B **106**, 7919 (2002).
29. G. Cuniberti, L. Craco, D. Porath and C. Dekker, Phys. Rev. B **65**, 241314 (2002).
30. G.C. Liang, A.W. Ghosh, M. Paulsson and S. Datta, Phys. Rev. B **69**, 115302 (2004).
31. M. Zwolak and M. Di Ventra, Appl. Phys. Lett. **81**, 925 (2002).
32. X.F. Wang and T. Chakraborty, Phys. Rev. B **74**, 193103 (2006).
33. I. Saito, T. Nakamura, K. Nakatani, Y. Yoshioka, K. Yamaguchi and H. Sugiyama, J. Am. Chem. Soc. **120**, 12686 (1998).
34. V.M. Apalkov and T. Chakraborty, Phys. Rev. B **71**, 033102 (2005).
35. E. Maciá and R. Rodriguez-Oliveros, Phys. Rev. B **74**, 144202 (2006).
36. N. Sutin, Prog. Inorg. Chem. **30**, 441 (1983).
37. Y.A. Berlin, A.L. Burin and M.A. Ratner, Chemical Physics **275**, 61 (2002).
38. In the literature, both t and $-t$ have been used as the coupling parameter. In Ref. [83], the transfer matrix formalism is presented assuming the coupling parameters t and λ, and has a different form than in this chapter.
39. M.A. Ratner, J. Phys. Chem. **94**, 4877 (1990).
40. P. Carpena, P. Bernaola-galvan, P. Ch. Ivanov and H.E. Stanley, Nature, **418**, 955 (2002); ibid. **421**, 764 (2003).
41. S. Roche and E. Maciá, Mod. Phys. Lett. B **18**, 847 (2004).
42. S. Datta, Quantum Transport: atom to transistor, Cambridge University Press, (2005).

43. F.D. Lewis, X. Liu, J. Liu, S.E. Miller, R.T. Hayes and M.R. Waslelewski, Nature, **406**, 51 (2000).
44. B. Giese, J. Amaudrut, A. Köhler, M. Spormann and S. Wessely, Nature **412**, 318 (2001).
45. M. Taniguchi and T. Kawai, Physica E **33**, 1 (2006).
46. D. Porath, A. Bezryadin, S. de Vries and C. Dekker, Nature **403**, 635 (2000).
47. S. Priyadarshy, S.M. Risser and D.N. Beratan, JBIC, **3**, 196 (1998).
48. J. Jortner, M. Bixon, T. Langenbacher and M.E. Michel-Beyerle, Proc. Natl. Acad. Sci. **95**, 12759 (1998); M. Bixon, B. Giese, S. Wessely, T. Langenbacher, M.E. Michel-Beyerle and J. Jortner, Proc. Natl. Acad. Sci. **96**, 11713 (1999).
49. B. Giese, Acc. Chem. Res. **33**, 631 (2000).
50. V.D. Lakhno, V.B. Sultanov and B.M. Pettitt, Chem. Phys. Lett. **400**, 47 (2004).
51. E. Meggers, M.E. Michel-Beyerle and B. Giese, J. Am. Chem. Soc. **120**, 12950 (1998).
52. Y.A. Berlin, A.L. Burin and M.A. Ratner, J. Phys. Chem. A **104**, 443 (2000).
53. H.M. McConnell, J. Chem. Phys. **35**, 508 (1961).
54. J.R. Reimers and N.S. Hush in electron transfer in biology and the solid state, Advances in Chemistry series Vol. 226, M.K. Johnson, R.B. King, D.M. Kurtz, C. Kutal, M.L. Norton and R.A. Scott, American Chemical Society, Washington, DC (1990), page 27.
55. J. Olofsson and S. Larsson, J. Phys. Chem. B **105**, 10398 (2001).
56. J. Jortner, M. Bixon, A.A. Voityuk and N. Rösch, J. Phys. Chem. A **106**, 7599 (2002).
57. K. Senthilkumar, F.C. Grozema, C.F. Guerra, F.M. Bickelhaupt, F.D. Lewis, Y.A. Berlin, M.A. Ratner and L.D.A. Siebbeles, J. Am. Chem. Soc. **127**, 14894 (2004).
58. A.K. Felts, W.T. Pollard and R.A. Friesner, J. Phys. Chem. **99**, 2929 (1995).
59. A. Okada, V. Chernyak and S. Mukamel, J. Phys. Chem. A **102**, 1241 (1998).
60. W.B. Davis, M.R. Wasielewski, M.A. Ratner, V. Mujica and A. Nitzan, J. Phys. Chem. A **101**, 6158 (1997).
61. J. Yi, Phys. Rev. B **68**, 193103 (2003).
62. H. Yamada, Int. J. Mod. Phys. B **18**, 1697 (2004).
63. K. Iguchi, J. Phys. Soc. Jpn. **70**, 593 (2001).
64. D. Klotsa, R.A. Römer and M.S. Turner, Biophys. J. **89**, 2187 (2005).
65. H. Basch, R. Cohen and M.A. Ratner, Nano Lett. **5**, 1668 (2005); H. Basch and M.A. Ratner, J. Chem. Phys. **123**, 234704 (2005).
66. F. Zahid, M. Paulsson, E. Polizzi, A.W. Ghosh, L. Siddiqui and S. Datta, J. Chem. Phys. **123**, 064707 (2005).
67. J.L. D'Amato and H.M. Pastawski, Phys. Rev. B **41**, 7411 (1990).
68. X.Q. Li and Y.J. Yan, Appl. Phys. Lett. **79**, 2190 (2001).
69. C.J. Murphy and M.R. Arkin, Y. Jenkins, N.D. Ghatlia, S.H. Bossman, N.J. Turro and J.K. Barton, Science **262**, 1025 (1993).
70. F.D. Lewis, T.F. Wu, Y.F. Zhang, R.L. Letsinger, S.R. Greenfield and M.R. Wasielewski, Science **277**, 673 (1997).
71. S.O. Kelley and J.K. Barton, Science **283**, 375 (1999).
72. R.N. Barnett, C.L. Cleveland, A. Joy, U. Landman and G.B. Schuster, Science **294**, 567 (2001).
73. M. Bixon and J. Jortner, Chemical Physics **281**, 293 (2002).

74. J. Jortner, M. Bixon, A.A. Voityuk and N. Rösch, J. Phys. Chem. A **106**, 7599 (2002).
75. T. Renger and R.A. Marcus, J. Phys. Chem. A **107**, 8404 (2003).
76. T. Cramer, S. Krapf and T. Koslowski, J. Phys. Chem. B **108**, 11812 (2004); M. Rateitzak and T. Koslowski, Chem. Phys. Lett. **377**, 455 (2003); N. Utz and T. Koslowski, Chem. Phys. **282**, 389 (2002).
77. D.M. Basko and E.M. Conwell, Phys. Rev. Lett. **88**, 098102 (2002); Phys. Rev. B **66**, 094304 (2002).
78. T. Holstein, Ann. Phys. **8**, 325 (1959); **8** 343 (1959).
79. W.P. Su, J.R. Schrieffer and A.J. Heeger, Phys. Rev. Lett. **42**, 1698 (1979); Phys. Rev. B **22**, 2099 (1980).
80. G.B. Schuster, Acc. Chem. Res. **33**, 253 (2000).
81. P.T. Henderson, D. Jones, G. Hampikian, Y.Z. Kan and G.B. Schuster, Proc. Natl. Acad. Sci. **96**, 8353 (1999).
82. P. Maniadis, G. Kalosakas, K.Ø. Rasmussen and A.R. Bishop, Phys. Rev. B **68**, 174304 (2003); S. Komineas, G. Kalosakas and A.R. Bishop, Phys. Rev. E **65**, 061905 (2002).
83. X.F. Wang and T. Chakraborty, Phys. Rev. Lett. **97**, 106602 (2006).
84. P.F. Barbara, T.J. Meyer and M.A. Ratner, J. Phys. Chem. **100**, 13148 (1996).
85. X.F. Wang and I.C. da Cunha Lima, Phys. Rev. B **63**, 205312 (2001).
86. V. Apalkov and T. Chakraborty, Phys. Rev. B 72, 161102 (2005).
87. L.I. Glazman and R.I. Shekhter, Zh. Eksp. Teor. Fiz. **94**, 292 (1987) Sov. Phys. JETP **67**, 163 (1988).
88. A. Mitra, I. Aleiner and A.J. Millis, Phys. Rev. B **69**, 245302 (2004).
89. M. Galperin, M.A. Ratner and A. Nitzan, J. Chem. Phys. **121**, 11965 (2004).
90. J. Koch and F. von Oppen, Phys. Rev. Lett. **94**, 206804 (2005).
91. L.P. Kouwenhoven, D.G. Austing and S. Tarucha, Rep. on Prog. Phys. **64**, 701 (2001).
92. S. Komineas, G. Kalosakas and A.R. Bishop, Phys. Rev. E **65**, 061905 (2002).
93. S. Luryi, Appl. Phys. Lett. **47**, 490 (1985).
94. F. Marsiglio, Physica C **244**, 21 (1995).
95. A. La Magna and R. Pucci, Phys. Rev. B **53**, 8449 (1996).
96. A.S. Alexandrov and N.F. Mott, Rep. Prog. Phys. **57**, 1197 (1994).
97. E.B. Starikov, Phil. Mag. Lett. **83**, 699 (2003).
98. A. La Magna and R. Pucci, Phys. Rev. B **55**, 14886 (1997).
99. E.M. Conwell and S.V. Rakhmanova, Proc. Natl. Acad. Sci. USA. **97**, 4556 (2000).
100. S.V. Rakhmanova and E.M. Conwell, J. Phys. Chem. B **105**, 2056 (2001).
101. V. Apalkov and T. Chakraborty, Phys. Rev. B **73**, 113103 (2006).
102. C.A.M. Seidel, A. Schulz and H.M. Sauer, J. Phys. Chem. **100**, 5541 (1996).
103. X. Hu, Q. Wang, P. He and Y. Fang, Anal. Sci. **18**, 645 (2002).
104. E.M. Conwell and D.M. Basko, J. Am. Chem. Soc. **123**, 11441 (2001).
105. A. Omerzu, M. Licer, T. Mertelj, V.V. Kabanov and D. Mihailovic, Phys. Rev. Lett. **93**, 218101 (2004).
106. J. Koch, M.E. Raikh and F. von Oppen, Phys. Rev. Lett. **96**, 056803 (2006).